

# Design, Synthesis, Characterization, and Crystal Structure Studies of Nrf2 Modulators for Inhibiting Cancer Cell Growth In Vitro and In Vivo

Prathima Chikkegowda,<sup>‡‡</sup> Baburajeev C. Pookunoth,<sup>‡‡</sup> Venugopal R. Bovilla,<sup>‡‡</sup> Prashanthkumar M. Veeresh, Zonunsiami Leihang, Thippeswamy Thippeswamy, Mahesh A. Padukudru, Basavanagowdappa Hathur, Rangappa S. Kanchugarakoppal, Basappa,<sup>\*</sup> and SubbaRao V. Madhunapantula<sup>\*</sup>



Cite This: <https://doi.org/10.1021/acsomega.0c06345>



Read Online

ACCESS |



Metrics & More

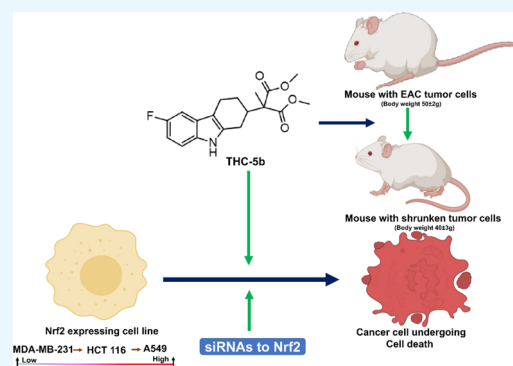


Article Recommendations



Supporting Information

**ABSTRACT:** Nrf2 is one of the important therapeutic targets studied extensively in several cancers including the carcinomas of the colon and rectum. However, to date, not many Nrf2 inhibitors showed promising results for retarding the growth of colorectal cancers (CRCs). Therefore, in this study, first, we have demonstrated the therapeutic effect of siRNA-mediated downmodulation of Nrf2 on the proliferation rate of CRC cell lines. Next, we have designed, synthesized, characterized, and determined the crystal structures for a series of tetrahydrocarbazoles (THCs) and assessed their potential to modulate the activity of Nrf2 target gene NAD(P)H:quinone oxidoreductase (NQO1) activity by treating colorectal carcinoma cell line HCT-116. Later, the cytotoxic potential of compounds was assessed against cell lines expressing varying amounts of Nrf2, viz., breast cancer cell lines MDA-MB-231 and T47D (low functionally active Nrf2), HCT-116 (moderately active Nrf2), and lung cancer cell line A549 (highly active Nrf2), and the lead compound **5b** was tested for its effect on cell cycle progression in vitro and for retarding the growth of Ehrlich ascites carcinomas (EACs) in mice. Data from our study demonstrated that among various compounds **5b** exhibited better therapeutic index and retarded the growth of EAC cells in mice. Therefore, compound **5b** is recommended for further development to target cancers.



## INTRODUCTION

Global cancer statistics have positioned cancer in the second place among various noncommunicable diseases as the total number of deaths due to cancers has reached ~10 million in the year 2018 worldwide. Among various cancers, breast and lung carcinomas (~2 million cases each in the year 2018) are the major ones contributing significantly to the total deaths due to cancers.<sup>1</sup> Likewise, colorectal cancer (CRC) is another major malignancy in men (third most common) and women (second most common) globally.<sup>2</sup> The number of deaths due to CRC has increased approximately to 694 000 worldwide, making CRC the fourth most common one among different cancer types.<sup>3</sup> Even though colorectal cancers are detected in the early age of life, the incidence (~90% of total cases) is more in individuals aged 50 years or above.<sup>4</sup> However, recently, a rising trend has been reported in the incidence rates of breast and colorectal cancers even among the younger individuals.<sup>5</sup>

In general, cancers are progressive diseases.<sup>6</sup> Early detection and effective therapeutic interventions help to mitigate cancers in a better manner. However, currently, not many sensitive

early detection markers exist for identifying breast, lung, and colorectal cancers.<sup>7</sup> For instance, CRC occurs over decades from early development of adenomatous precursor lesions to invasive metastatic stages.<sup>8</sup> Early stages of CRC are curable by surgical resection and chemotherapy; however, the advanced malignant stages are difficult to treat. The chemotherapeutic drugs commonly used in the therapy of CRC are 5-fluorouracil (5-FU), oxaliplatin, capecitabine, and irinotecan.<sup>9</sup> Recently, US-FDA has approved targeted therapies such as bevacizumab, cetuximab (Erbix), and panitumumab for the treatment of CRCs. Bevacizumab prevents angiogenesis in the tumor by targeting vascular endothelial growth factor (VEGF). Along with cetuximab (Erbix) and panitumumab, which interfere with cancer cell growth by targeting the epidermal growth

**Received:** December 30, 2020

**Accepted:** March 24, 2021

**A**

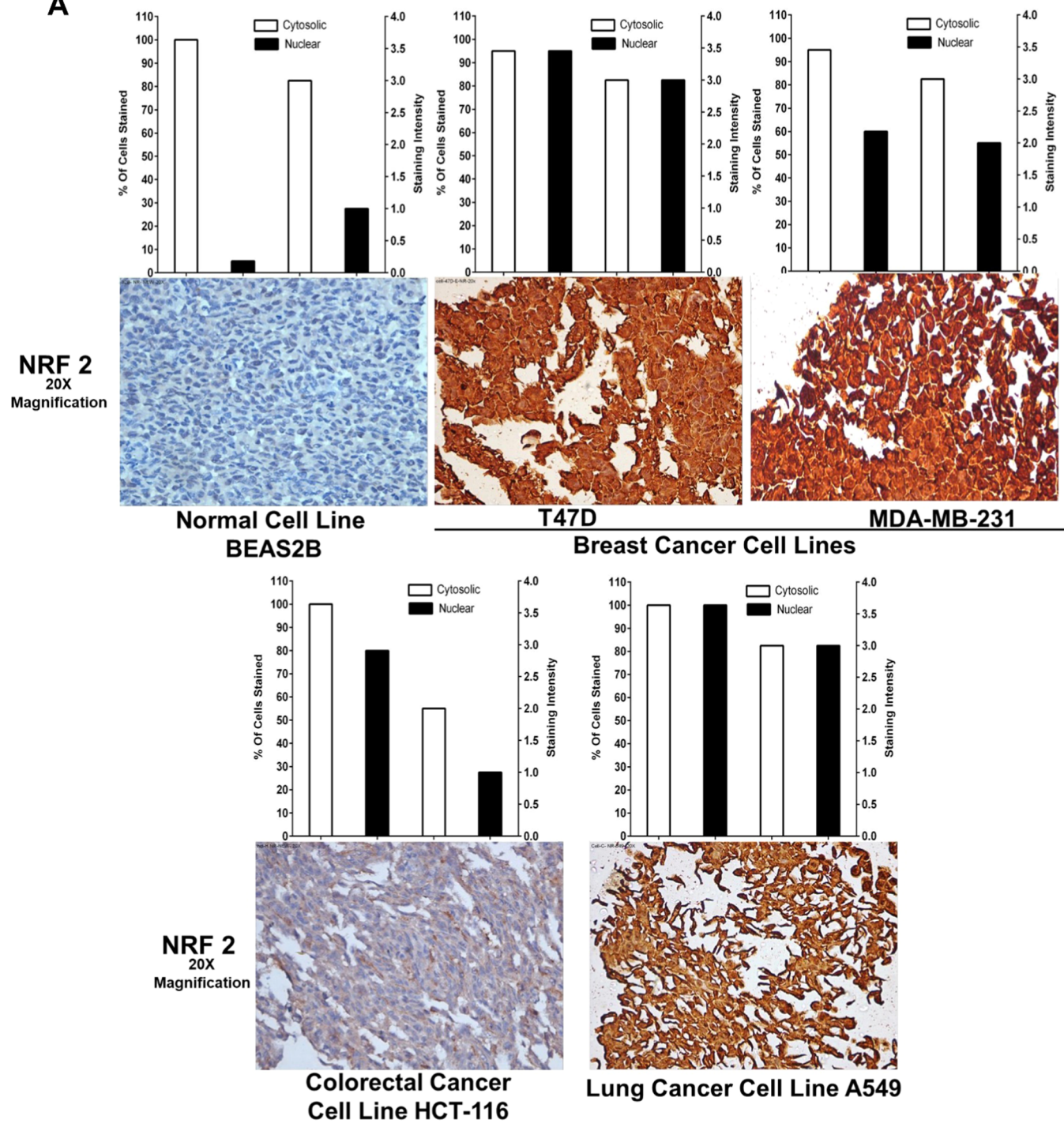
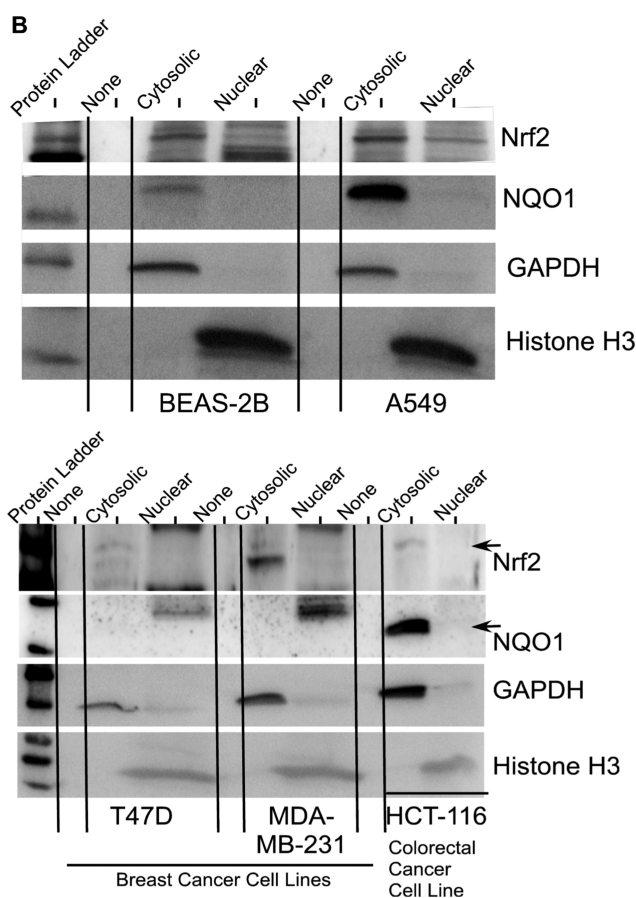


Figure 1. continued



**Figure 1.** Cancer cell lines exhibited variations in the expression of Nrf2 compared to normal lung epithelial cell line BEAS-2B. To determine the expression level and cellular localization status of Nrf2 and its downstream target NQO1, first, immunocytochemical (ICC) analysis was carried out on cell blocks prepared as detailed in section [Experimental Section](#). (A) Elevated Nrf2 expression in cancer cell lines compared to that in normal cell line BEAS-2B. The expressed Nrf2 is primarily localized in the nuclei of cancer cells (A). Unlike ICC, the analysis of nuclear and cytosolic fractions using western blotting showed elevated cytosolic and nuclear Nrf2 in the A549 cell line compared to that in BEAS-2B (B, top panel). However, the breast and colorectal carcinoma cell lines showed expression of Nrf2 only in the cytosol (B, bottom panel). Nrf2 target protein NQO1 is expressed in the cytosol of lung and colorectal cancer cell lines but not in breast cancer cell lines (B). Very low NQO1 was detected even in normal lung epithelial cell line BEAS-2B (B, top panel).

factor receptor (EGFR) or proteins involved in tumor development, bevacizumab showed a better therapeutic effect against CRCs.<sup>10</sup> However, certain tumors with genetic mutations (like EGFR, K-RAS, or B-RAF) fail to respond to these drugs, especially, cetuximab or panitumumab.<sup>11</sup> Thus, more effective strategies for early intervention and treatment are in high demand for better management of breast, lung, and colorectal carcinomas.<sup>11</sup>

In this direction, identification of key proteins regulating cancer cell growth and metastasis is very critical for the development of more effective, potent, nontoxic, targeted therapies to inhibit breast, lung, and colorectal cancers. One such important target recently identified in various cancers is nuclear factor (erythroid-derived 2)-like 2, also known as NFE2L2 or Nrf2.<sup>12</sup> While activators of Nrf2 prevents the transformation of normal cells to cancer cells, the inhibitors of Nrf2 help in sensitizing the tumor cells to radiation and chemotherapeutic agents.<sup>13</sup> Nrf2 is one of the important regulators of redox status in cells. Under normal conditions, Nrf2 is kept in its inactive state by Keap1; however, when cells are exposed to oxidative stress, Keap1 undergoes polyubiquitination and degradation by the 26S proteasome pathway to release Nrf2.<sup>14</sup> Thus, Keap1 is a negative regulator of Nrf2.<sup>15,16</sup> Once released from Keap1, Nrf2 translocates to the nucleus

and binds to the antioxidant response element (ARE) in the promoter regions of various genes involved in controlling oxidative stress.<sup>17,18</sup> For instance, Nrf2-induced activation of antioxidant and phase II-detoxification target genes such as heme oxygenase 1 (HO1),  $\gamma$ -glutamyl cysteine synthetase (catalytic subunit; GCLC), glutathione reductase, glutathione peroxidase (GPx), thioredoxin reductase, and peroxiredoxins is well reported.<sup>19</sup> Upon re-establishment of cellular redox homeostasis, Keap1 translocates to the nucleus to dissociate Nrf2 from the ARE, resulting in the degradation of Nrf2.<sup>20,21</sup> Overall, Nrf2 is an important transcription factor of the antioxidant response and a good sensor of cellular redox status.<sup>22</sup> Hence, activation of Nrf2 is essential to prevent the transformation of normal cells to cancer cells.<sup>23,24</sup>

However, paradoxically, Nrf2 behaves as a “double-edged” sword in cancers.<sup>25,26</sup> Overexpression of Nrf2 has been reported in many cancers including the breast, colon, rectum, and lung carcinomas.<sup>27</sup> Elevated Nrf2 in cancer cells protects tumors from chemotherapeutic agents as well as radiation-induced damage.<sup>27</sup> Therefore, targeting Nrf2 is one of the important strategies for treating cancers where Nrf2 plays a vital role in tumorigenesis and drug resistance. In this direction, efforts have been made by many investigators to purify and or synthesize novel compounds to either promote

the activity of Nrf2 in normal cells or to inhibit the Nrf2 and its target genes in cancer cells.<sup>28</sup> For example, natural chemopreventive agents such as carotenoids, curcumins, cyclic lactones, diterpenes, dithiolethiones, epithionitriles, flavonoids, indoles, isothiocyanates, organosulfides, and phenols that induce the Nrf2 pathway and thereby prevent the transformation of normal cells to cancer cells have been purified and characterized by many investigators.<sup>29</sup> A recent study demonstrated that induction of Nrf2 using pharmacological agents protected the colon from inflammation-induced cancer.<sup>27</sup> Besides protecting normal cells from oxidative stress and chemotherapeutic drugs, Nrf2 also extends its protective effects even on cancer cells, thereby promoting tumor growth.<sup>30,31</sup> Therefore, targeted inhibition of Nrf2 in tumor cells is highly essential for retarding tumors.<sup>32</sup> However, to date, not many Nrf2-modulating pharmacological agent(s) showed better anticancer activity in preclinical animal models and clinical trials. Possible reasons for the minimal success of Nrf2 modulators in preclinical and clinical trials are (a) poor selectivity, (b) systemic toxicity, (c) lack of acceptable pharmacokinetic and dynamic properties, and (e) very low bioavailability.

Carbazoles are a set of bioactive heterocyclic systems known to exhibit anticancer effects.<sup>33</sup> Carbazole-based heterocycles are known to exhibit potent anticancer, antimicrobial, antiretroviral (HIV), antiarthritic, antidiabetic, and anticancer activities.<sup>33,34</sup> For example, novel carbazole analogues have been shown to exhibit antitumor activity in triple-negative breast cancer cells by inhibiting STAT3 signaling followed by the induction of protein tyrosine phosphatase 6.<sup>35</sup> Carbazoles and their derivatives inhibit cancer growth by intercalating into DNA, inhibiting DNA topoisomerase II activity, and by forming covalent DNA adducts.<sup>34</sup> Different natural and synthetic carbazole derivatives including ellipticine, olivacine, elliptinium acetate, mahanimbine, mukonine, koenoline, and rebaccamycin have been reported to exhibit antineoplastic activity.<sup>35</sup> A carbazole compound LCY-2-CHO was reported to inhibit NO production in microglia.<sup>36</sup> In continuation of these studies, and our research on developing biologically important heterocyclic compounds,<sup>37–39</sup> we now reported the synthesis of a series of tetrahydrocarbazole derivatives as Nrf2 modulators and demonstrated the cytotoxic potential of Nrf2-modulating tetrahydrocarbazoles. Further, the potential of the most potent Nrf2 modulator was tested *in vivo* for its ability to retard Ehrlich ascites carcinoma (EAC) tumors in mice.

## RESULTS AND DISCUSSION

**Nrf2 is a Key Therapeutic Target in Breast, Colorectal, and Lung Carcinomas.** To determine whether Nrf2 is a key therapeutic target in cancers, first, the expression and activity of Nrf2 (in terms of its target gene NQO1 function) were compared in cell lines representing breast, lung, colon, and rectum carcinomas with those of normal platelets. Analysis of Nrf2 expression using immunocytochemistry (ICC) showed a very high Nrf2 in all cancer cell lines compared to that in normal lung epithelial cell line BEAS-2B (Figure 1A). Subcellular localization analysis by measuring the number of cells stained and the intensity of staining score showed variations among cancer cell lines. The normal cell line BEAS-2B had a very low staining intensity score both in the cytosol and nucleus (Figure 1A). Among different cancer cell lines, the ones representing breast carcinoma (T47D and MDA-MB-231) and the one representing lung carcinoma (A549) had

staining intensity scores of 2 or above, both in the cytosol and nuclear regions, which are higher compared to that of colorectal cancer cell line HCT-116 (Figure 1A). To test further this data and provide a more accurate assessment, next, the distribution of Nrf2 in the cytosol and nucleus was estimated using a method (detailed in the Experimental Section), which separates these two fractions with purity. Experimentally, the cytosolic and nuclear fractions were collected and analyzed by western blotting (Figure 1B, top panel). Analysis of the data showed that Nrf2 was expressed predominantly in the cytosol of normal lung epithelial cell line BEAS-2B and lung carcinoma cell line A549. However, only the A549 nuclear fraction showed Nrf2 expression, indicating the differential distribution of Nrf2 in normal and cancer cell lines. This data is in good correlation with the ICC analysis, wherein the intensity of staining was very low in the nuclear region of the BEAS-2B cell line compared to that in the A549 cell line (Figure 1A). Interestingly, Nrf2 is localized in the cytosolic region in breast (MDA-MB-231 and T47D) and colorectal (HCT-116) carcinoma cell lines (Figure 1B, bottom panel). This data correlates well with ICC analysis of MDA-MB-231 and HCT-116 cell lines for Nrf2 expression (Figure 1A). However, in the case of T47D, a discrepancy was observed when the Nrf2 expression was compared between ICC and western blotting. Whereas ICC analysis showed more nuclear staining, the analysis by western blotting showed no nuclear expression (compare Figure 1A with Figure 1B, bottom panel). Further studies using immunofluorescence and confocal microscopy examination might help in addressing this discrepancy. Nrf2 target gene NQO1 expression was observed only in the cytosolic fraction of all of the cell lines tested. NQO1 was almost undetectable in T47D and MDA-MB-231 breast cancer cell lines (Figure 1B, bottom panel). Next, to check whether the expressed Nrf2 is functionally active or is just expressed, the NQO1 activity in breast, lung, and colorectal cancer cell lines was compared to that in normal platelet cells (Table 1). NQO1 is a well-reported direct target

**Table 1. Comparison of NQO1 Activity of Colorectal (HCT-116) and Lung (A549) Carcinoma Cell Lines, Breast Cancer Cell Lines (T47D and MDA-MB-231), and Normal Platelets<sup>a</sup>**

name of the cell line	NQO1 activity ( $\mu\text{mol}/\text{min}/\text{mg}$ protein)
platelets	0.47 $\pm$ 0.63
T47D	16.06 $\pm$ 2.02
MDA-MB-231	14.36 $\pm$ 6.50
HCT-116	152.79 $\pm$ 5.09
A549	243.24 $\pm$ 14.16

<sup>a</sup>To determine the NQO1 activity, which is an indicator of functionally active Nrf2, protein lysates were collected as detailed in section Experimental Section and NQO1 activity was estimated. Analysis of the data showed that breast carcinoma cell lines T47D and MDA-MB-231 had very low NQO1 activity compared to colorectal carcinoma cell line HCT-116 (moderate activity) and lung carcinoma cell line (A549). Human platelets had very low NQO1 activity.

of Nrf2, hence an indicator of functionally active Nrf2. The level of NQO1 activity was much higher in colorectal (HCT-116) and lung (A549) cancer cell lines compared to that in breast (T47D and MDA-MB-231) cancer cell line as well as normal platelets (Table 1), which is in good correlation with

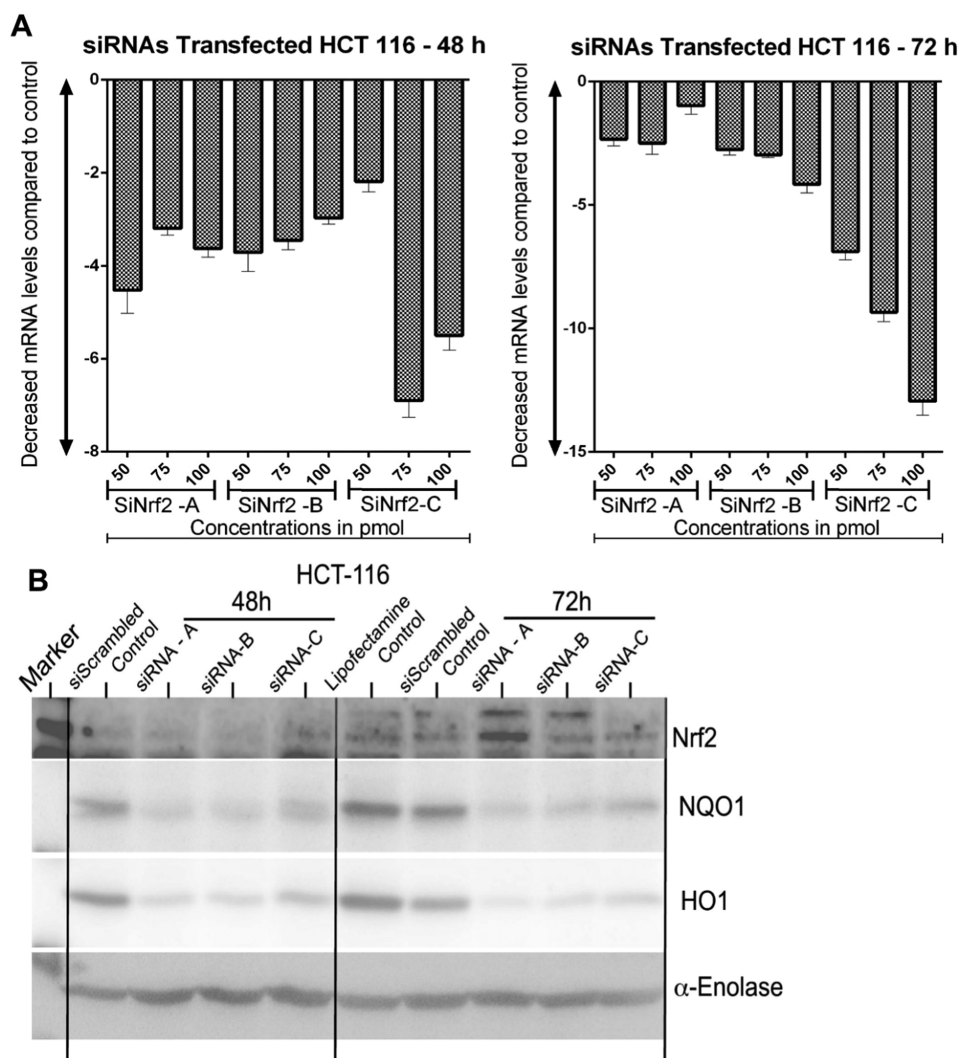


**Figure 2.** SiRNAs targeting Nrf2 reduced the expression of Nrf2 mRNA and protein in HCT-116 cells. To test and determine the efficacy of siRNAs targeting Nrf2, HCT-116 cells were transfected with Lipofectamine RNAi Max containing 50, 75, and 100 pmol siRNA (each separately) and total RNA isolated after 48 and 72 h. The isolated RNA was used to synthesize cDNA, and Nrf2 expression was measured using RT-PCR. SiRNAs-A and -B showed a moderate decrease in Nrf2 compared to siRNA-C (A). Visible decrease in Nrf2 and its targets HO1 and NQO1 protein was also observed upon knocking down Nrf2 using siRNAs (B).

the western blotting data, wherein the expression of NQO1 was almost undetectable in T47D and MDA-MB-231 cell lines.

**Targeted Inhibition of Nrf2 Using siRNAs Retarded Cancer Cell Proliferation In Vitro.** The effect of targeted inhibition of Nrf2 on cell proliferation was determined by transfecting specific siRNAs. Experimentally, Nrf2 expression was reduced by transfecting the cells with validated stealth siRNAs (refer to Supporting Information Table S1 for siRNA sequences) (from Invitrogen), followed by measuring the Nrf2 expression at the mRNA level after 48 and 72 h of transfection (Figure 2A and Table 2). Procedurally, HCT-116 cells were transfected with siRNAs targeting Nrf2 and control scrambled siRNA using lipofectamine RNAi Max reagent, as detailed in section Experimental Section. Total RNA was isolated from control and transfected cells; fold change in target gene expression due to siRNA transfection was determined using formula  $2^{-\Delta\Delta CT}$ , where  $\Delta\Delta CT = (CT \text{ of the gene of interest in the test sample} - CT \text{ of internal control of the test sample}) - (CT \text{ gene of the interest control sample} - CT \text{ internal control of the control sample})$ . A significant decrease in Nrf2

**Table 2.** Effect of Transfecting Nrf2 siRNAs Using Lipofectamine RNAi Max Reagent on the  $C_t$  Value of Nrf2 and Housekeeping Gene GAPDH

cells transfected with	$C_t$ (cycle threshold) value of target gene	
	Nrf2	GAPDH *
no reagent	17.62	11.75
DEPC water	16.31	11.35
SiScramble	17.09	11.44
SiNrf2-A	20.08	11.12
SiNrf2-B	20.80	12.00
SiNrf2-C	22.80	11.46

expression at the mRNA level was observed due to siRNA introduction into HCT-116 cells (Table 2), indicating the efficacy of targeted siRNAs in knocking down Nrf2 (Figure 2A). For instance, an about 8.5- and 7.6-fold decrease in Nrf2 mRNA expression was observed with 100 pmol siRNA-A and siRNA-B, respectively, at 72 h. Interestingly, siRNA-C yielded a 14-fold decrease in Nrf2 expression compared to siScrambled control (Figure 2A). Further analysis of knockdown cells for

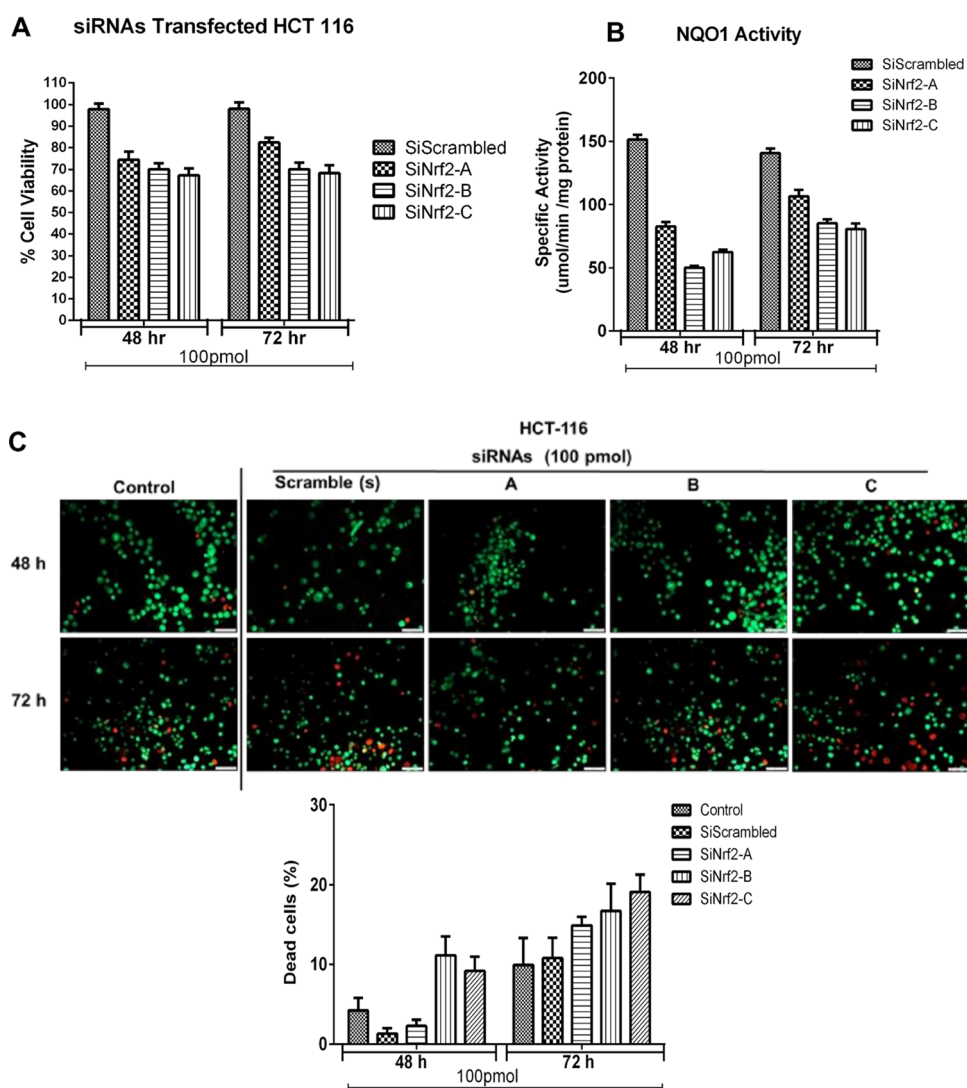


**Figure 3.** Targeted inhibition of Nrf2 expression using siRNA reduced cell viability, decreased NQO1 activity, and promoted cell death in the HCT-116 cell line. Targeted inhibition of Nrf2 reduced the viability (A) and NQO1 activity (B) in HCT-116 cells compared to scrambled siRNA transfected cells ( $P < 0.05$ ; by one-way analysis of variance (ANOVA)). A significant increase in the number of dead cells was also observed with Nrf2 knockdown in HCT-116 cell line (C).

the expression of Nrf2 and its target proteins HO1 and NQO1 using western blotting showed an about 2–3-fold decrease in Nrf2 protein with siRNA-A, -B, and -C at 48 and 72 h (Figure 2B). Targeted inhibition of Nrf2 reduced cell proliferation by nearly 30% (Figure 3A) with a significant 2–3-fold decrease in NQO1 activity, indicating the potential of siRNAs for reducing Nrf2 and its target gene NQO1 activity while decreasing cell proliferation (Figure 3B).

**Genetic Ablation of Nrf2 Using siRNAs Reduced the Number of Viable Cells by Promoting Cell Death in HCT-116 Cell Line.** Since HCT-116 cells had moderately elevated Nrf2, next, the effect of targeted inhibition of Nrf2 expression on cell proliferation and NQO1 activity was determined by counting the number of total cells after 48 h of transfection (Figure 3A,B). Analysis of the data showed a significant decrease (12.5–21.0%) in the total number of viable cells compared to siScrambled control (Figure 3A). A much better knockdown was observed when the comparison was made with DEPC-treated control (30.0–37.0%). A significant reduction in NQO1 activity was also observed at 48 h (~50–66%) and 72 h (30–50%) post-transfection,

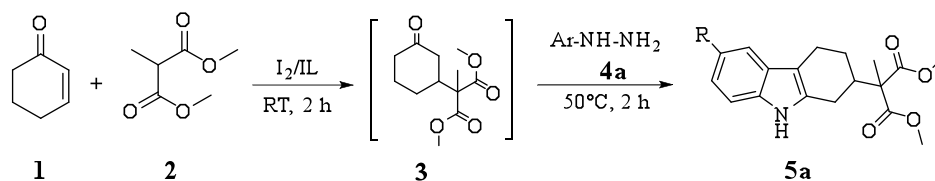
indicating further that transfection of HCT-116 cells using siRNAs reduced the expression of Nrf2 (Figure 3B). In summary, targeted inhibition of Nrf2 reduced the viability of colorectal carcinoma cell line HCT-116 (Figure 3A and Table 3).

To check whether the reduced cell number is because of increased cell death, the transfected cells were incubated with acridine orange and ethidium bromide, and the stained cells

**Table 3. Knocking Down Nrf2 Retarded Cell Proliferation In Vitro**

cells transfected with	total cell number ( $0.5 \times 10^6$ )	% inhibition (compared to siScramble)	% inhibition (compared to DEPC water)
no reagent	0.76	no inhibition	15.0
DEPC water	0.9	no inhibition	0.00
siScramble	0.72	0.00	20.0
siNrf2-A	0.58	19.0	35.0
siNrf2-B	0.57	21.0	37.0
siNrf2-C	0.63	12.5	30.0

## Scheme 1. Synthesis of Dimethyl-2-methyl-2-(6-substituted-2,3,4,9-tetrahydro-1H-carbazol-2-yl) Malonates



were observed under a fluorescence microscope (Figure 3C). A significant 2–3-fold increase in the number of dead cells was observed upon transfecting HCT-116 cells with siRNA to Nrf2 (Figure 3C). The percentage of dead cells was much higher at 72 h compared to 48 h post-transfection (Figure 3C).

In summary, targeted knockdown of Nrf2 using siRNAs reduced colorectal cancer cells by promoting cell death through the reduction of Nrf2 expression and its target genes NQO1 and HO1. Hence, Nrf2 is a potential therapeutic target in cancers; hence, developing pharmacological agents for inhibiting Nrf2 expression could be a viable strategy for mitigating cancers.

**Design, Method Development, Synthesis, and Characterization of Tetrahydrocarbazoles.** Since targeted inhibition of Nrf2 in cancer cells reduced the number of cells through cell death induction, and the fact that the carbazole-based compounds inhibit NO production, we herein synthesized tetrahydrocarbazoles, which possess a bent structure, by Borsche–Drechsel (BD) cyclization in the presence of iodine catalyst in ionic liquid (IL) media.<sup>40,41</sup> We applied a multicomponent reaction procedure and an ionic liquid as a medium to obtain a green protocol, where the liberation of volatile organic solvents was prevented. ILs offer several advantages that include high boiling point, negligible vapor pressure, high thermal stability, and good solvating ability of catalysts.<sup>42</sup> A recent study on BD cyclization, which utilized iodine via Michael addition<sup>42</sup> in IL media prompted us to carry out the one-pot iodine-catalyzed synthesis of dimethyl-2-(3-substituted-6,7,8,9-tetrahydro-5H-carbazol-7-yl)-2-methyl malonates (THCs).

The reaction condition was optimized by, first, beginning the one-pot synthesis of dimethyl-2-(3-substituted-6,7,8,9-tetrahydro-5H-carbazol-7-yl)-2-methylmalonate **5a** using cyclohexene-1-one **1**, 2-methyl dimethylmalonate **2**, *p*-chlorophenylhydrazine **4a** in the presence of molecular iodine, and iodobenzenediacetate at different conditions (Supporting Information Table S2). First, the reaction in the presence of iodine catalyst but in the absence of the solvent produced required product **5a** in 60% yield (entry 1, Supporting Information Table S2). This reaction when carried out on solid support (alumina) also generated the same product, however, in lower yield (43% compared to the one carried out using iodine catalyst) (entry 2, Supporting Information Table S2). The reaction in ILs 1-butyl-3-methylimidazolium tetrafluoroborate ([BMIM][BF<sub>4</sub>]), 1-ethyl-3-methylimidazolium tetrafluoroborate (EMIMBF<sub>4</sub>), 1-ethyl-3-methylimidazolium bromide ([EMIM]Br), and 1-methyl-3-propylimidazolium bromide ([PMIM]Br) yielded **5a** in about 87–91% yield (entries 3–6, Supporting Information Table S2). When the reaction was conducted in the presence of iodobenzenediacetate in the absence of the solvent, solid support (alumina), [BMIM]BF<sub>4</sub>, EMIMBF<sub>4</sub>, [EMIM]Br, and [PMIM]Br gave **5a** in 25–72% yields (entries 7–12, Supporting Information Table S2). Notably, the reaction in the absence of any catalyst

yielded no product (entry 13, Supporting Information Table S2). Thus, a maximum yield of 91% was obtained in [BMIM][BF<sub>4</sub>] (entry 3, Supporting Information Table S2) (Scheme 1).

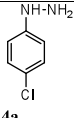
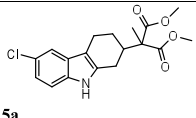
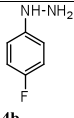
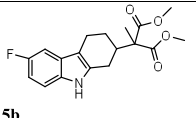
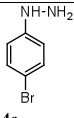
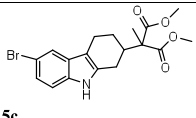
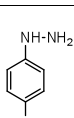
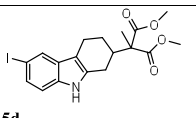
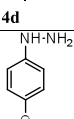
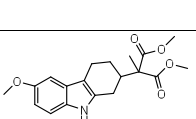
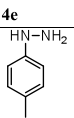
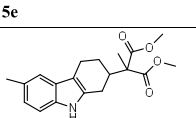
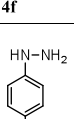
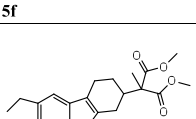
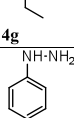
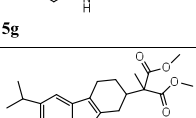
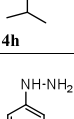
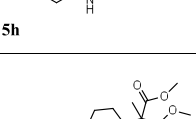
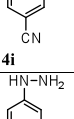
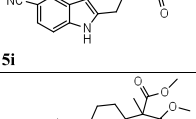
With the optimized reaction conditions in hand, we next synthesized a set of diverse THCs (Table 4). Reaction of different aryl hydrazines **4b–k** substituted with halogens (Cl, F, Br, I), methoxy, methyl, ethyl, isopropyl, cyano, and nitro groups yielded respective THCs **5a–l** in about 45–91% yields. The mechanisms leading to the formation of THCs are well established.<sup>42</sup> One of the THCs **5a** was analyzed by single-crystal X-ray diffraction study of at 50% probability confirmed its structure and its ORTEP diagram is shown in Supporting Information Figure S1. Its crystallographic data is deposited at Cambridge Crystallographic Data Centre as supplementary publication CCDC-1019396.

**Novel Tetrahydrocarbazoles Interact with the Nrf2–Keap1 Attachment Region by Binding to Keap1 Protein.** To test whether THCs modulate the expression and activity of Nrf2, first, the THC derivatives were docked at the interface of Keap1–Nrf2. The observed binding poses of the docking studies revealed that THCs play an important role in selective binding to the Keap1–Nrf2 interface region (Figure 4A,B).

Molecular docking studies showed that THCs bind to Keap1 via  $\pi$ -cation interaction of its aromatic scaffold with Arg415. In addition, hydrogen bonding was also observed with Ser363, Ser508, or Ser555. Further, the salt bridge interaction between the negatively charged groups of THCs and Arg380, Arg415, or Arg483 was also noticed. The interaction of **5b** with target Nrf2–Keap1 interface (the interaction map and surface view) is shown in Figure 4. It is now hypothesized that THCs might be stabilizing the molecular interactions between Keap1 and Nrf2, thereby preventing the translocation of Nrf2 to the nucleus. Cytosolic Nrf2 is inactive and, hence, failed to extend protection against oxidative stress, leading to cell death.<sup>43</sup> However, this hypothesis requires additional studies to provide experimental evidence.

**Cytotoxic Potential of THCs against Cancer Cell Lines HCT-116, A549, MDA-MB-468, and MDA-MB-231 Depends on the Level of Nrf2 Expression.** To test whether Nrf2–Keap1 interaction-stabilizing THCs exhibit cytotoxic potential against cell lines expressing low, moderate, and very high Nrf2, i.e., MDA-MB-231 and MDA-MB-468, HCT-116, and A549, respectively, a dose–response cytotoxicity study was conducted using the methyl thiazolyl tetrazolium (MTT) assay. THCs with chloro and fluoro substituents **5a** and **5b**, respectively, had IC<sub>50</sub> values of 92.58 and 159.60  $\mu$ M in the HCT-116 cell line (Table 5 and Figure 5A). Other THCs had IC<sub>50</sub> greater than 100  $\mu$ M against the HCT-116 cell line. For instance, THCs **5d** and **5h** with iodo- and isopropyl groups are inactive and no inhibition is observed even at 100  $\mu$ M concentration. Unlike the HCT-116 cell line when tested against A549, which had very high functionally active Nrf2,

**Table 4. Synthesis of 2-Methyl-2-(6-substituted-2,3,4,9-tetrahydro-1H-carbazol-2-yl) Malonates**

Entry	Ar-NH-NH <sub>2</sub> <b>4</b>	Product <b>5</b>	Time (h)	Yield (%)
1	 <b>4a</b>	 <b>5a</b>	4	91
2	 <b>4b</b>	 <b>5b</b>	4	90
3	 <b>4c</b>	 <b>5c</b>	4	89
4	 <b>4d</b>	 <b>5d</b>	4	91
5	 <b>4e</b>	 <b>5e</b>	4	91
6	 <b>4f</b>	 <b>5f</b>	4	87
7	 <b>4g</b>	 <b>5g</b>	4	90
8	 <b>4h</b>	 <b>5h</b>	4	88
9	 <b>4i</b>	 <b>5i</b>	5	45
10	 <b>4j</b>	 <b>5j</b>	5	51

THCs **5a–j** had an  $IC_{50}$  lower than  $50 \mu\text{M}$ . Among various THCs, chloro-substituted Compound **5b** exhibited better cytotoxic potential with an  $IC_{50}$  of  $45.90 \mu\text{M}$  when tested against the A549 cell line (Figure 5A). In general, THCs are more active on A549, which expressed two times more Nrf2 than HCT-116.

**Compound 5b Elevated NQO1 Activity in HCT-116 Cells.** To check whether the cytotoxic effect exhibited by **5b** is due to the inhibition of Nrf2, the NQO1 activity was measured

in protein lysates collected from HCT-116 and A549 cell lines exposed to 31.25, 62.5, 125, and  $250 \mu\text{M}$  **5b** compound. Interestingly, the NQO1 activity was elevated with compound treatment (Figure 5B). Currently, it is unknown how Keap1–Nrf2 interaction-stabilizing **5b** promotes NQO1 activity. Further studies are warranted to check whether **5b** is also binding to NQO1, thereby promoting its activity through the stabilization of active conformation. Analysis of the protein lysates collected from the control and compound **5b**-treated cells showed a visible increase in p27 compared to control untreated cells (Figure 5C). Similarly,  $200 \mu\text{M}$  naringenin, a known activator of Nrf2, also increased p27 expression in the A549 cell line (Figure 5C). However, interestingly, the inhibitor of Nrf2, i.e., Brusatol, did not elevate p27 expression but slightly reduced the NQO1 level in A549 cells (Figure 5C). Furthermore, treatment of A549 cells with compound **5b** marginally increased the expression of proliferation marker Cyclin-D1, and apoptosis inducer Bax (Figure 5C). In summary, results of western blot analysis showed a significant increase in p27 expression upon treatment with compound **5b**.

**Compound 5b-Mediated Cell Proliferation Inhibition Is Mediated by G0/G1 Cell Cycle Arrest in HCT-116 and A549 Cells.** To elucidate the mechanism of cell proliferation inhibition caused by compound **5b**, Nrf2-expressing HCT-116 and A549 cells were exposed to increasing concentrations of **5b** for 24 and 48 h, and effect on cell cycle progression was studied, as detailed in Methods. Analysis of the data showed a visible increase in G0/G1 population upon treatment with compound **5b** of HCT-116 (Figure 6A) and A549 (Figure 6B). A moderate increase in Sub-G0/G1 (an indicator of apoptosis) was also observed in both cell lines treated with compound **5b** (Figure 6). Positive control Brusatol ( $500 \text{ nM}$ ) arrested cells in the S-phase while decreasing the cell count in G0–G1. Apoptotic cell percentage also increased upon treatment with Brusatol (Figure 6A,B). Many pharmacological agents that trigger p27 expression reported to induce cell cycle arrest in the G0–G1 phase. For instance, Moon et al. reported G0/G1 cell cycle arrest with a simultaneous increase in p27 (Kip1) by a compound panaxydol.<sup>44</sup> Similarly, many other studies have also shown upregulation of p27 and G0–G1 cell cycle arrest upon treatment with pharmacological agents that inhibit the Nrf2 signaling pathway.<sup>45,46</sup> A proof-of-principle study demonstrated that targeted downregulation of Nrf2 using siRNA induced G0/G1 cell cycle arrest in human lung cancer cell line A549 (Homma et al., 2009).<sup>47</sup> Based on these reports and our initial observations, we now conclude that treating HCT-116 and A549 cell lines with compound **5b** induced cell cycle arrest in the G0–G1 phase through Nrf2 inhibition followed by p27 upregulation.

**Cytotoxic THCs Inhibited Nrf2-Expressing EAC Cell Proliferation in Mice.** To determine the efficacy of lead compound **5b** in retarding the growth of Ehrlich ascites carcinoma (EAC) cells, first, the EAC cells were injected into the peritoneal cavity of mice, and after 24 h, the animals were treated intraperitoneally with **5b** at  $10 \text{ mg/kg}$  body weight (Figure 7). The dose was selected based on a pilot study, which demonstrated no toxicity at this concentration (data not shown). After 2 weeks, the animals were sacrificed and body weight, ascites fluid volume, and cell count determined (Figure 7A–D). Under these experimental conditions, compound **5b** decreased the body weight by two fold (Figure 7A,C). A significant decrease in the total cell count and ascitic fluid volume was noticed upon administering **5b** (Figure 7D).



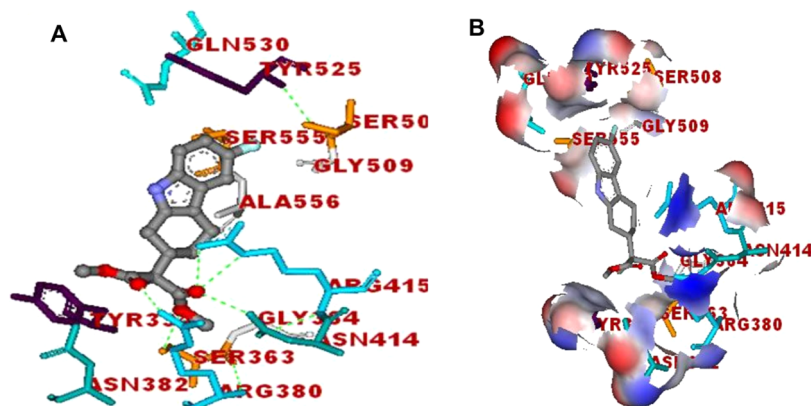


**Figure 4.** Molecular docking of THC<sub>s</sub> in Keap1 protein. In silico molecular docking experiments showed that compound **5b** interacts with the Nrf2–Keap1 interface: (A) Interaction map and (B) surface view of compound **5b** (stick model, green) and its surface-bound view with the protein–protein interface.

**Table 5.** IC<sub>50</sub> Values of THC<sub>s</sub> and Their C-Docker and C-Docker Interaction Energies

S	IC <sub>50</sub> (μM)		C-Docker energy	C-Docker interaction energy
	HCT-116	A549		
Sa	92.58	49.4	22.701	32.598
Sb	<b>159.60</b>	<b>45.9</b>	22.621	33.979
Sc	253.3	25.2	22.759	31.175
Sd	NA	47.4	23.613	36.344
Se	553	29.1	20.019	30.94
Sf	148.8	23.4	23.443	32.742
Sg	115.7	30.5	20.861	30.429
Sh	NA	23.8	24.029	33.691
Si	199.2	25.5	21.285	32.688
Sj	395.1	24.4	21.348	35.014

Sodium butyrate (24 mg/kg body weight), which was used as a positive control, showed a 2.5–3.0-fold decrease in the body weight compared to untreated and vehicle dimethyl sulfoxide (DMSO)-treated animals. The EAC model is a well-established breast cancer model to study the pharmacological action of anticancer agents.<sup>48,49</sup> Previously, we have shown the use of this model to test the efficacy of anticancer agents.<sup>50</sup> In addition, we have also demonstrated that EAC cells express elevated Nrf2 signaling; hence, they are a suitable model cell for testing the potency of Nrf2 inhibitors in vivo.<sup>51,52</sup> As predicted, compound **5b** retarded the growth of Nrf2-expressing EAC tumors in animals. A prior study showed the efficacy of derivatives synthesized by hybridization of THC<sub>s</sub> with dithioate against colorectal carcinoma cell lines in vitro.<sup>53</sup> Apart from this study, no other studies have reported the efficacy of THC<sub>s</sub> in inhibiting tumor cells. Therefore, the results presented in this article are novel and contribute to the development of potent antitumor agents for inhibiting carcinomas, where Nrf2 has a role in cell proliferation, cell survival, and drug resistance. Since targeting Nrf2 is one of the viable approaches for inhibiting tumor cell growth and metastasis, compound **5b**, which is reported in this study, is likely to provide key structural insights for further development of selective antitumor agents.

## CONCLUSIONS

In conclusion, data of our study showed (a) elevated expression of Nrf2 in colorectal and lung carcinoma cell lines

compared to that in breast cancer cells as well as normal lung epithelial cells, (b) the efficacy of targeted inhibition of Nrf2 using siRNA in retarding cancer cell proliferation, (c) an optimized scheme for the synthesis of tetrahydrocarbazole **5b**, (d) the potency of compound **5b** to inhibit cancer cell lines expressing moderate and high Nrf2 compared to the ones with low Nrf2, and (e) the safety and efficacy of compound **5b** for retarding Ehrlich ascites carcinomas in mice. Therefore, we conclude that compound **5b** may be considered for further development to treat cancers.

## EXPERIMENTAL SECTION

**General.** MTT powder (from Sisco Research Laboratories Pvt. Ltd., Mumbai, Maharashtra, India) was dissolved in phosphate-buffered saline (PBS) at a concentration of 10 mg/mL, and the solution was filtered through a 0.2 μm filter and stored at 2–8 °C for further use or frozen for extended periods. Ten microliters of stock MTT was added to each well containing 200 μL of media (the final concentration of MTT is 0.5 mg/mL). CellTiter 96 Aqueous MTS reagent powder and phenazine methosulfate (PMS) were procured from Promega Corporation, Madison, WI and Merck KGaA, Darmstadt, Germany, respectively. Cell lines MDA-MB-231, MDA-MB-468, T47D, HCT-116, and A549 were procured from the National Center for Cell Science, Pune, Maharashtra, India. Tissue culture-grade flasks T25 and T75, 96-well and 6-well plates, 100 mm Petri plates, and serological pipettes were from Techno Plastic Products Pvt. Ltd., Bengaluru, Karnataka, India.

**Measurement of NQO1 Activity.** NQO1 activity was measured by incubating glucose-6-phosphate (G6P) with glucose-6-phosphate dehydrogenase (G6PDase) followed by utilizing the produced NADPH to reduce menadiol into menadiol.<sup>54</sup> Menadiol thus produced reduces MTT to a blue formazan, which is measured at 562 nm in an Eppendorf spectrophotometer. The assay was performed as described by Prochaska et al.<sup>55</sup> Dicoumarol was used to measure the background activity contributed by other reductases. First, the culture medium was removed, and cells were washed two times with PBS. Next, the cells were scraped and washed with PBS. To the cell pellet, 500 μL of lysis buffer containing NP-40 and 2 mM ethylenediaminetetraacetic acid (EDTA) was added and mixed well. The cells were incubated for 30 min in the cell lysis buffer and the total protein content was estimated using Pierce BCA protein estimation kit.

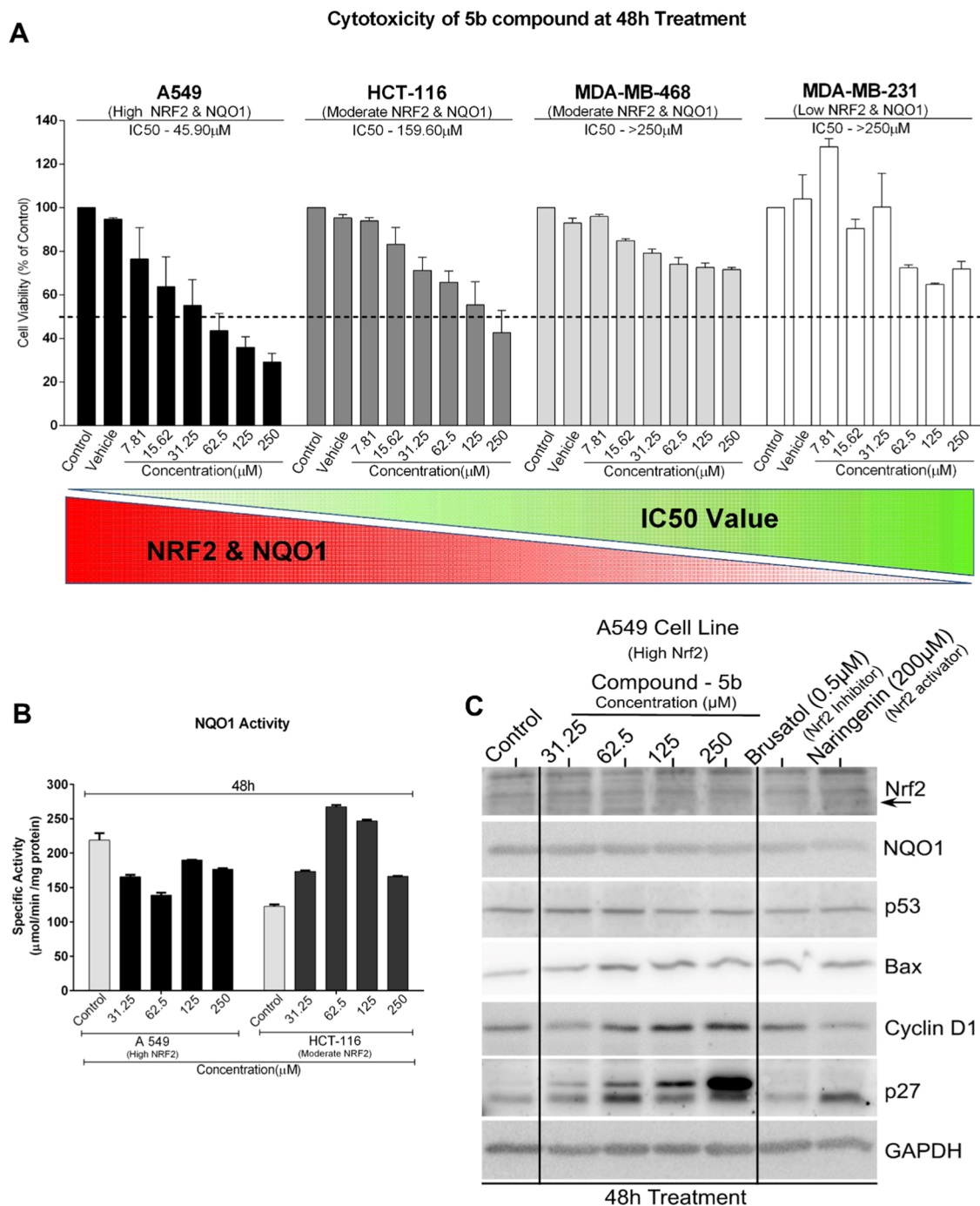


**Figure 5.** Compound **5b** reduced the proliferation of HCT-116 and A549 cells in vitro by promoting the expression of cell cycle inhibitor p27. Compound **5b** inhibited the proliferation of A549, HCT-116, MDA-MB-231, and MDA-MB-468 cells in a dose-dependent fashion (A). Interestingly treatment with compound **5b** increased NQO1 activity till 62.5  $\mu\text{M}$  (B). However, doses higher than 62.5  $\mu\text{M}$  might be toxic; hence, a reduction in NQO1 activity was reported. Compound **5b** induced the expression of p27 in the Nrf2-expressing A549 cell line, indicating that cell growth inhibition induced by compound **5b** could be in part due to elevated cell cycle arrest mediated by p27 expression (C).

**Preparation of NQO1 Cocktail for NQO1 Activity Analysis.** NQO1 cocktail was prepared by mixing the reagents listed in Supporting Information Table S3. Note that two sets of tubes, one containing dicoumarol and the other one without dicoumarol, were prepared for each measurement.

**Assay.** Ten micrograms of total protein (collected from the cells) in a total volume of 40  $\mu\text{L}$  was incubated with 200  $\mu\text{L}$  of NQO1 cocktail containing or not containing dicoumarol (3 with dicoumarol + 3 without dicoumarol). The absorbance was

read at 610 nm for a period of 30 min with 1 min interval (refer to Supplementary Methods for calculations).

**siRNA-Mediated Knockdown of Nrf2 Using Lipofectamine RNAi Max Reagent.** Knockdown of Nrf2 was achieved by transfecting  $1 \times 10^6$  HCT-116 cells with 25 pmol (2.5  $\mu\text{L}$  from 10  $\mu\text{M}$  stock) validated stealth siRNAs (three sets of siRNAs targeting different regions of Nrf2 gene—from Invitrogen, Thermo Fisher Scientific India Pvt. Ltd., Maharashtra, India) using Lipofectamine RNAi Max reagent (7.5  $\mu\text{L}$ ) as recommended by the supplier. The siRNA

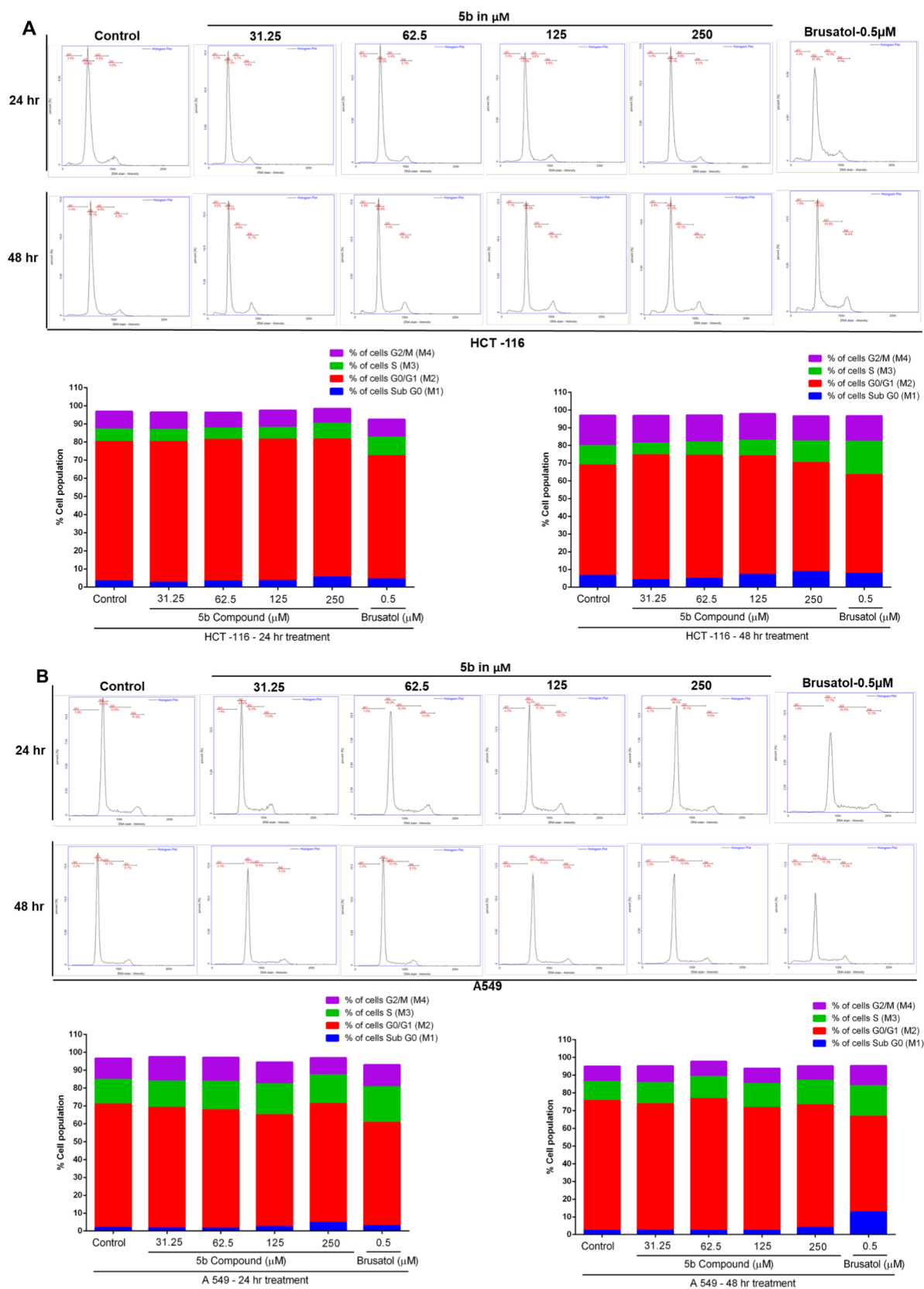


**Figure 6.** Compound **5b** induced cell cycle arrest in the G0–G1 phase in HCT-116 and A549 cells. To further test whether cell proliferation inhibition caused by compound **5b** treatment is due to cell cycle arrest, Nrf2-expressing HCT-116 (A) and A549 (B) cells were treated with 31.25, 62.5, 125, and 250  $\mu$ M compound **5b** for 24 and 48 h and cell cycle progression was determined, as detailed in [Experimental Section](#). A visible increase in G0–G1 population was observed in both cell lines upon treatment with compound **5b**.

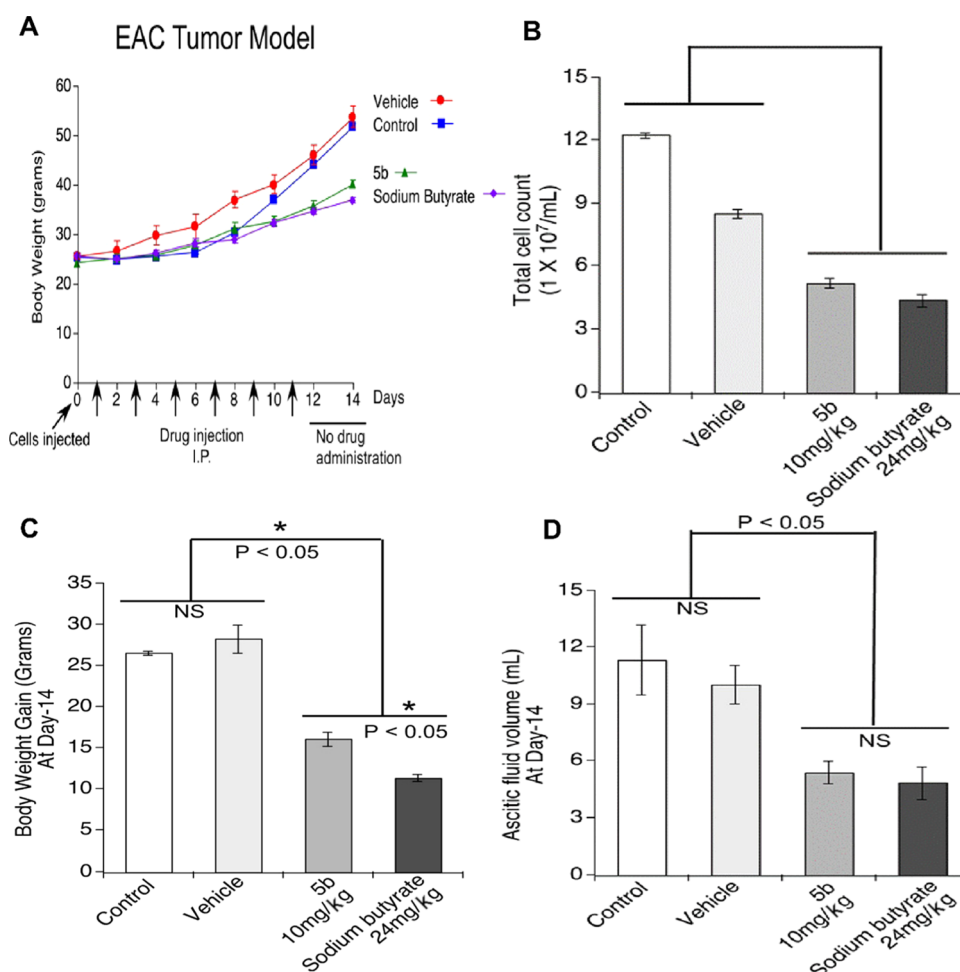


**Figure 7.** Intrapertoneal administration of compound **5b** inhibited EAC cell growth in mice. The efficacy of compound **5b** in inhibiting EAC cell growth in mice was studied as detailed in [Experimental Section](#). The data showed a significant decrease in the body weight (an indicator of tumor inhibition): (A) tumor cells count (B), body weight gain (C), and ascites fluid volume (D). In summary, compound **5b** is a potent inhibitor of tumor growth in mice.

sequence is provided in Supporting Information [Table S1](#). The level of knockdown at 24, 48, 72, and 96 h was determined using real-time polymerase chain reaction (PCR). In addition, the number of cells was counted and plotted to check whether targeted inhibition of Nrf2 has any effect on cell proliferation. Furthermore, the MTS assay was carried out to estimate the effect on cell viability as detailed in Madhunapantula et al.<sup>56</sup> Experimentally, MTS (stock concentration 2 mg/mL in PBS) and PMS (stock concentration 0.92 mg/mL in PBS) were mixed in 20:1 ratio and 20  $\mu$ L of reagent was added to 100  $\mu$ L of media. After addition, the plate was incubated in a CO<sub>2</sub> incubator for 1–2 h and the absorbance was read at 470 nm.

**Isolation of Total RNA from Cells.** Total RNA from cultured cells was isolated using the Trizol (guanidiniumisothiocyanate–phenol–chloroform mixture) method.<sup>57</sup> The quality of isolated RNA was checked using 1% bleach gel by measuring the ratio between 28S and 18S bands. The quality of isolated RNA is rated good when the ratio between 28S and 18S bands is 2:1.<sup>58</sup> Quantification of human NRF2 and other genes was performed using the DyNAmo Color Flash SYBR Green QPCR Kit by following the manufacturer's instructions. Experimentally, first, the reaction mixture, in a total volume of 20  $\mu$ L, containing 50 ng of template cDNA and primers was prepared in each tube. The samples were analyzed in duplicate

to determine the reproducibility. Following primers were used for the analysis of expression of NRF2 and its downstream genes.

**NRF2 (According to Zou X. et al.).** Forward primer: TTCAGCAGCATCCTCTCCACAG

Reverse primer: GCATGCTGTTGCTGATACTGG

**GAPDH (Internal Control for Normalization).** Forward primer: CGACCACTTTGTCAAGCTCA

Reverse primer: AGGGGAGATTTCAGTGTGGTG

Fold change due to treatment =  $2^{-\Delta\Delta Ct}$ , where  $\Delta\Delta Ct = (CT \text{ of the gene of interest in the test sample} - CT \text{ of internal control of the test sample}) - (CT \text{ gene of the interest control sample} - CT \text{ internal control of the control sample})$ .

**Analysis of the Expression of Nrf2 and Its Target Genes HO1 and NQO1 and Proliferation and Apoptosis Markers Using Western Blotting.** To determine the impact of knocking down Nrf2 on its target genes HO1 and NQO1 protein expression, cell lysates were collected and analyzed on 10% NuPAGE gels as detailed in Madhunapantula et al.<sup>59</sup> Total protein quantity was determined using the BCA assay.<sup>60</sup> About 50  $\mu$ g of total protein/well was loaded and analyzed as described in Madhunapantula et al.<sup>59</sup> Expression of Nrf2, HO1, NQO1 and p53, Bax, Cyclin-D1, and P27 was measured by detecting the respective proteins using primary antibodies

recognizing Nrf2 (cat no. 12721), NQO1 (cat no. 62262), HO1 (cat no. 5853), p53 (cat no. 9282S), Bax (cat no. D2E11), Cyclin-D1 (cat no. SC718), and P27 (cat no. SC 393380) obtained from Cell Signaling Technologies, Danvers, MA. Enolase (cat no. SC-7455) and secondary antibodies (antirabbit and antigoat) conjugated with horseradish peroxidase (HRP; rabbit cat no. SC2357 and goat cat no. SC2020) were from Santacruz Biotechnology, Dallas, TX. The proteins were detected using ECL (Western Bright ECL cat no. K-12045-D20), Advansta Corporation, San Jose, CA.

#### Preparation of Cytosolic and Nuclear Extracts.

Cytosolic and nuclear extracts were prepared from cell lines BEAS-2B, A549, T47D, MDA-MB-231, and HCT-116 as detailed by Baghirova et al.<sup>61</sup> After 48 h of growth at 37 °C in a CO<sub>2</sub> incubator, the culture medium was removed and washed with PBS twice to remove the media components. Next, the cells were trypsinized and approximately 3 × 10<sup>6</sup> cells were pelleted by centrifugation. The cell pellet was washed with ice-cold PBS (500 μL) and resuspended in 400 μL of ice-cold lysis buffer "A" (150 mM NaCl, 50 mM *N*-(2-hydroxyethyl)-piperazine-*N'*-ethanesulfonic acid (HEPES) pH 7.4, 25 μg/mL Digitonin, and 1 M glycerol) supplemented with protease inhibitor cocktail (1%, Sigma-Aldrich, St. Louis, MI). The reaction mixture was kept for incubation on an end-over-end rotator for 30 min at 4 °C. Cytosolic proteins were collected by centrifugation of the reaction mixture at 2000g for 10 min at 4 °C. The pellet was resuspended in 400 μL of ice-cold lysis buffer "B" (150 mM NaCl, 50 mM HEPES pH 7.4, 1% NP-40, and 1 M glycerol) supplemented with protease inhibitor cocktail from Sigma-Aldrich, St. Louis, MI). The reaction mixture was vortexed for 30 s and incubated on ice for 30 min with 15 s vortexing at every 10 min interval. Now, at this point, the membrane-bound proteins were collected by centrifugation at 7000g for 10 min at 4 °C. To the remaining pellet, 400 μL of ice-cold lysis buffer "C" (150 mM NaCl, 50 mM HEPES pH 7.4, 0.5% sodium deoxycholate, 0.1% sodium dodecyl sulfate (SDS), and 1 M glycerol) supplemented with protease inhibitor cocktail from Sigma-Aldrich, St. Louis, MI). The reaction mixture was incubated on the end-over-end rotator for 30 min at 4 °C to allow complete solubilization of nuclei. Centrifugation was carried out at 7800g for 10 min at 4 °C, and the supernatant that contained the nuclear protein was collected in a fresh 1.5 mL centrifuge tube. Total protein in the collected fractions was estimated using BCA and analyzed on 10% polyacrylamide gel electrophoresis (PAGE) gel. The purity of cytosolic and nuclear fractions was tested by probing with GAPDH (a cytosolic protein) and Histone-H3 (a nuclear protein).

**Determination of Cell Viability Using the MTT/MTS Assay.** First, a stock of 12 mM MTT was prepared by adding 1 mL of sterile PBS to 5 mg of MTT, and a stock of 10% SDS in 0.01 M HCl (1 g of SDS in 10 mL of 0.01 M HCl) was prepared. Next, 10 μL of 12 mM MTT was added to cells (untreated and treated) growing in 100 μL of complete medium lacking phenol red. The plate was incubated for 4 h in a CO<sub>2</sub> incubator at 37 °C and centrifuged at 200 rpm for 5 min, and the supernatant was removed. To each well, 100 μL of 10% SDS solution was added to dissolve the pharazine crystals that were formed due to viable cells. The absorbance was measured at 570 nm in a multimode plate reader.

**Assessment of Cell Death Using Acridine Orange and Ethidium Bromide Staining.** The number of cells undergoing cell death was detected by a double staining procedure

using acridine orange and ethidium bromide as described by Shailasree et al.<sup>62</sup> Experimentally, 0.3 × 10<sup>6</sup> HCT-116 cells transfected with scrambled siRNA and siRNA targeting Nrf2 in 2.0 mL of media/well were plated in six-well plates and allowed to grow for 48 and 72 h. The untreated control and cells transfected with siRNA were trypsinized and mixed thoroughly to obtain a single-cell suspension. Trypsin was neutralized by the addition of complete medium, and 20.0 μL of cell suspension was incubated with 10.0 μL of 100.0 mg/mL ethidium bromide and 10.0 μL of 100.0 mg/mL acridine orange mixture for 5.0 min. The cells were imaged using TRITC and FITC filters of a fluorescence microscope. The images obtained using 2.0 different channels were later merged to obtain a combined image, which exhibited green live cells and orange dead cells.

**Impact of Compound 5b Treatment on Cell Cycle Stages.** To determine the variations in cell cycle stages upon treatment with compound 5b, a two-step cell cycle assay using 4',6-diamidino-2-phenylindole (DAPI) was used. Since DAPI preferentially binds to double-stranded DNA and the contribution by DAPI/RNA complex is only about 20% of that of the DAPI/DNA complex, no RNA digestion is required in this assay.<sup>63</sup> The stained cells were quantified using a NucleoCounter NC-3000 system.<sup>64,65</sup> Experimentally, about 1 × 10<sup>6</sup> were washed twice with PBS (500 μL each time) by centrifugation at 500g for 10 min and resuspended in 500 μL of PBS. Next, 500 μL of sample was added dropwise to 4.5 mL of ice-cold 70% ethanol while mixing the cells using a vortex mixture. The cell fixation was carried out for 2 h at 4 °C, and the cell suspension was centrifuged at 500g for 5 min. The ethanol supernatant was discarded carefully, and the cell pellet was washed with 5.0 mL of PBS by centrifugation at 500g for 5 min. The cell pellet was resuspended in 500 μL of solution 3 (1.0 μg/mL DAPI, 0.1% Triton X-100 in PBS). The cells were incubated in solution 3 for 5 min at room temperature, and an aliquot of 30 μL was loaded into NC-Slide A2 and analyzed using the Fixed Cell Cycle-DAPI Assay program of NC-3000.<sup>66</sup> The data was analyzed based on the number and intensity of DAPI-stained cells. Histograms were captured, and the percentage of cells in each cell cycle stage was determined. Brusatol 0.5 μM was used as a positive control in this assay.

**Efficacy of Compound 5b to Inhibit EAC Cells In Vitro.** The cytotoxic potential of compounds 5b was determined by the trypan blue dye exclusion method. In brief, first, EAC cells were cultured in peritoneal cavity of healthy albino mice by injecting a suspension 1 × 10<sup>6</sup> EAC cells/mL.<sup>67</sup> On day 15, the cells were aspirated aseptically from the peritoneal cavity of the mice and washed with normal saline by centrifugation for 15 min at 1500 rpm in a refrigerated centrifuge. The pellet was resuspended with normal saline, and the process was repeated until a clear supernatant was obtained. Finally, the cells were suspended in normal saline, and the cell count was adjusted to 1 × 10<sup>6</sup> cells/mL. Then, 0.1 mL of this cell suspension was distributed into Eppendorf tubes and exposed to 0.1 mL of increasing concentrations of compounds 5b for 3 h at 37 °C. The trypan blue dye exclusion test was performed to determine the cytotoxicity percentage.<sup>68</sup> Trypan blue is a diazo dye that selectively stains dead cells and thereby helps in identifying and differentiating the live and dead cells.<sup>68</sup>

**Efficacy of Selected Compounds for Inhibiting EAC Cells Growing in Mice. Acute Toxicity Study.** Animal toxicity study was conducted as per OECD guideline 423.<sup>69</sup>

No mortality or behavioral and morphological abnormalities were observed at the dose of 300 mg/kg of compound **5b**. Induction of EAC liquid tumor and the administration of selected compounds were carried out, described as follows:<sup>67</sup> The experiment was carried out as per the protocol approved by the Institutional Animal Ethics Committee of JSS Medical College, JSS Academy of Higher Education & Research, Mysuru. First, EAC cells were aspirated from the peritoneal cavity of EAC-bearing mice using an 18-gauge needle into a sterile syringe. The total number of viable cells/mL was counted by trypan blue staining, and the ascitic fluid suitably diluted in PBS to obtain  $10^7$  cells/mL. To induce ascitic tumor,  $2.5 \times 10^6$  cells (0.25 mL of stock suspension) were injected intraperitoneally to each mice ( $n = 6$  in each group). Treatment of mice with **5b** was started at a dose of 10 mg/kg after 24 h of tumor cell injection and continued for a total of 14 days.

**Molecular Docking Study.** The computational docking studies were carried out to understand the binding mode of THCs to the Nrf-Keap1 interface. The compounds were docked into the exposed protein–protein interface of Keap1–Nrf2 (PDB ID: 4iqk). We used Accelrys Product DS software and CDOCKER protocol for the molecular docking studies. The compound set was docked using the default setting of the CDOCKER program, and the affinity scoring function was made. The highest scoring pose for each compound, out of ten intermediate docking runs, set was identified for further studies.

**Statistical Analysis.** To determine the significance between two groups, a simple Student's *t*-test was carried out. However, to determine the significance among multiple groups, one-way analysis of variance (one-way ANOVA) was used. The "*p*" < 0.05 values were considered significant. All of the statistical analyses were carried out using Graph Pad Prism Version 5.0.

## SYNTHESIS AND CHARACTERIZATION OF TETRAHYDROCARBAZOLE COMPOUNDS

**General.** All solvents and reagents used were of analytical grade and purchased from Sigma-Aldrich, St. Louis, MI. Infrared spectra were obtained in KBr disc on a Shimadzu FT-IR 157 spectrometer. The <sup>1</sup>H and <sup>13</sup>C NMR spectra were recorded on a Bruker WH-200 (400 and 100 MHz, respectively) spectrometer in CDCl<sub>3</sub> or DMSO-*d*<sub>6</sub> as the solvent using TMS as an internal standard. Chemical shifts were expressed in ppm. Mass spectra were determined on an Agilent LC–MS. The progress of the reactions was monitored using precoated silica gel-G thin layer chromatography (TLC) plates. Melting points were recorded on a Selaco melting point apparatus.

**General Procedure for the Synthesis of THCs 5a–j.** To a stirred mixture of cyclohexene-1-one **1** (2 mmol) and 2-methyl dimethylmalonate **2** (2 mmol) in 1-butyl-3-methylimidazolium tetrafluoroborate ([BMIm][BF<sub>4</sub>], 2 mL), iodine (10 mol %) was added and stirred for 2 h. Completion of the reaction was monitored by thin-layer chromatography (TLC). Substituted phenylhydrazine (**4a–j**) (2 mmol) was added to the reaction mass and heated at 50 °C for 2 h. The solid obtained was filtered under vacuum and washed with diethyl ether. The obtained solid products (**5a–j**) were recrystallized in ethanol.

### DIMETHYL-2-METHYL-2-(3-OXOCYCLOHEXYL)-MALONATE 3

<sup>1</sup>H NMR (CDCl<sub>3</sub>, 400 MHz):  $\delta$  3.73 (s, 3H, OMe), 3.72 (s, 3H, OMe), 2.52–2.23 (m, 5H, CH, (CH<sub>2</sub>)<sub>2</sub>), 1.89–1.85 (m, 1H, CH), 1.74–1.62 (m, 2H, CH<sub>2</sub>), 1.49–1.42 (m, 4H, CH, CH<sub>3</sub>); DEPT-135 (100 MHz): 52.2, 52.6, 42.7, 16.9 (–OCH<sub>3</sub>, –CH, –CH<sub>3</sub>), 43.3, 41.1, 26.6, 24.7 (–CH<sub>2</sub>); <sup>13</sup>C NMR (CDCl<sub>3</sub>, 100 MHz):  $\delta$  210.2, 171.4, 56.9, 52.6, 52.5, 52.6, 43.3, 42.7, 41.1, 26.6, 24.7, 16.9; HRMS (ESI-TOF) *m/z*: [M + H]<sup>+</sup> calcd for C<sub>12</sub>H<sub>19</sub>O<sub>5</sub>, 243.1232 found, 243.1234.

### DIMETHYL 2-(6-CHLORO-2,3,4,9-TETRAHYDRO-1H-CARBAZOL-2-YL)-2-METHYLMALONATE 5A

<sup>1</sup>H NMR (CDCl<sub>3</sub>, 400 MHz):  $\delta$  7.72 (s, 1H, N–H), 7.40 (s, 1H, Ar–H), 7.18–7.16 (d, *J* = 8.8 Hz, 1H, Ar–H), 7.07–7.04 (d, *J* = 10.8, 1H, Ar–H), 3.767 (s, 3H, OMe), 3.748 (s, 3H, OMe), 2.82–2.62 (m, 5H, CH, (CH<sub>2</sub>)<sub>2</sub>), 2.053–2.012 (m, 1H, CH), 1.59–1.52 (m, 4H, CH, CH<sub>3</sub>); <sup>13</sup>C NMR (CDCl<sub>3</sub>, 100 MHz):  $\delta$  172.0, 171.9, 152.8, 135.2, 132.2, 110.5, 110.3, 109.1, 108.8, 103.1, 57.0, 52.5, 52.4, 39.6, 25.6, 25.2, 21.1, 16.0; HRMS (ESI-TOF) *m/z*: [M + H]<sup>+</sup> calcd for C<sub>18</sub>H<sub>20</sub>ClNO<sub>4</sub>, 350.1159 found, 350.1160.

### DIMETHYL 2-(3-FLUORO-6,7,8,9-TETRAHYDRO-5H-CARBAZOL-7YL)-2-METHYLMALONATE 5B

<sup>1</sup>H NMR (CDCl<sub>3</sub>, 400 MHz):  $\delta$  7.67 (s, 1H, NH), 7.19–7.18 (dd, *J*<sub>1</sub> = 5.76 Hz, *J*<sub>2</sub> = 5.76 Hz, 1H, Ar–H), 7.17–7.15 (dd, *J*<sub>1</sub> = 3.28 Hz, *J*<sub>2</sub> = 3.28 Hz, 1H, Ar–H), 6.68–6.89 (m, 1H, Ar–H), 3.77 (s, 3H, OMe), 3.75 (s, 3H, OMe), 2.84–2.67 (m, 5H, CH, (CH<sub>2</sub>)<sub>2</sub>), 2.07–2.05 (m, 1H, CH), 1.62–1.50 (m, 4H, CH, CH<sub>3</sub>); <sup>13</sup>C NMR (CDCl<sub>3</sub>, 100 MHz):  $\delta$  172.1, 172.0, 153.0, 135.0, 132.4, 110.8, 110.2, 109.2, 108.9, 103.2, 57.1, 52.6, 52.5, 39.7, 25.7, 25.1, 21.1, 17.0; HRMS (ESI-TOF) *m/z*: [M + H]<sup>+</sup> calcd for C<sub>18</sub>H<sub>21</sub>FNO<sub>4</sub>, 334.1455 found, 334.1457.

### DIMETHYL 2-(3-BROMO-6,7,8,9-TETRAHYDRO-5H-CARBAZOL-7YL)-2-METHYLMALONATE 5C

Brown solid; mp 130–131 °C. <sup>1</sup>H NMR (CDCl<sub>3</sub>, 400 MHz):  $\delta$  7.81 (s, 1H, NH), 7.50 (s, 1H, Ar–H), 7.28–7.25 (d, 1H, *J* = 12.0 Hz, 1H, Ar–H), 7.16–7.14 (d, 1H, *J* = 8.0 Hz, 1H, Ar–H), 3.76 (s, 3H, OMe), 3.74 (s, 3H, OMe), 2.81–2.67 (m, 5H, CH, (CH<sub>2</sub>)<sub>2</sub>), 2.04–2.02 (m, 1H, CH), 1.60–1.49 (m, 4H, CH, CH<sub>3</sub>); <sup>13</sup>C NMR (CDCl<sub>3</sub>, 100 MHz):  $\delta$  171.9, 152.5, 134.6, 128.5, 124.9, 121.3, 117.4, 111.3, 109.8, 108.9, 57.1, 52.5, 39.5, 25.6, 25.0, 21.0, 17.0, 16.9. HRMS (ESI-TOF) *m/z*: [M + H]<sup>+</sup> calcd for C<sub>18</sub>H<sub>21</sub>BrNO<sub>4</sub>, 394.0654 and 396.0633 found, 394.0656 and 396.0636.

### DIMETHYL 2-(3-iodo-6,7,8,9-tetrahydro-5H-carbazol-7-yl)-2-methylmalonate 5D

Yellow solid; mp 122–123 °C. <sup>1</sup>H NMR (CDCl<sub>3</sub>, 400 MHz):  $\delta$  7.69 (s, 1H, NH), 7.31 (s, 1H, Ar–H), 7.19–7.17 (d, *J* = 8.0 Hz, 1H, Ar–H), 7.08–7.06 (d, *J* = 8.0 Hz, 1H, Ar–H), 3.77 (s, 3H, OMe), 3.76 (s, 3H, OMe), 2.84–2.65 (m, 5H, CH, (CH<sub>2</sub>)<sub>2</sub>), 2.06–2.03 (m, 1H, CH), 1.57–1.50 (m, 4H, CH, CH<sub>3</sub>); <sup>13</sup>C NMR (CDCl<sub>3</sub>, 100 MHz):  $\delta$  171.9, 152.9, 134.5, 128.4, 124.8, 121.2, 117.4, 111.2, 109.7, 108.8, 57.0, 52.4, 39.5,

25.5, 24.9, 20.9, 17.0, 16.9; HRMS (ESI-TOF)  $m/z$ :  $[M + H]^+$  calcd for  $C_{18}H_{21}INO_4$ , 442.0515 found, 442.0518.

■ **DIMETHYL**  
**2-(6,7,8,9-TETRAHYDRO-3-METHOXY-5H-CARBAZOL-7YL)-2-METHYLMALONATE 5E**

White solid; mp 128–129 °C.  $^1H$  NMR ( $CDCl_3$ , 400 MHz):  $\delta$  7.70 (s, 1H, NH), 7.14 (s, 1H, Ar-H), 6.95–6.74 (dd,  $J_1 = 2.4$ ,  $J_2 = 2.4$ , 1H, Ar-H), 6.72–6.70 (m, 1H, Ar-H), 3.81 (s, 3H, OMe), 3.76 (s, 3H, OMe), 3.75 (s, 3H, OMe), 2.75–2.67 (m, 5H, CH,  $(CH_2)_2$ ), 2.04–2.01 (m, 1H, CH), 1.73–1.52 (m, 4H, CH,  $CH_3$ );  $^{13}C$  NMR ( $CDCl_3$ , 100 MHz):  $\delta$  172.3, 153.9, 137.4, 130.7, 127.8, 110.7, 110.6, 109.0, 108.7, 102.5, 58.5, 55.8, 52.8, 36.6, 27.3, 23.0, 20.4, 17.7, 16.8; HRMS (ESI-TOF)  $m/z$ :  $[M + H]^+$  calcd for  $C_{19}H_{24}NO_5$ , 346.1654 found, 346.1656.

■ **DIMETHYL**  
**2-(3-ETHYL-6,7,8,9-TETRAHYDRO-5H-CARBAZOL-7YL)-2-METHYLMALONATE 5G**

White solid; mp 121–122 °C.  $^1H$  NMR ( $CDCl_3$ , 400 MHz):  $\delta$  7.70 (s, 1H, NH), 7.14–7.12 (d,  $J = 8.0$  Hz, 1H, Ar-H), 6.95 (s, 1H, Ar-H), 6.75–6.72 (dd,  $J_1 = 7.4$  Hz,  $J_2 = 2.4$  Hz, 1H, Ar-H), 3.76 (s, 3H, OMe), 3.75 (s, 3H, OMe), 3.60–3.55 (m, 2H,  $CH_2$ ), 2.73–2.67 (m, 5H, CH,  $(CH_2)_2$ ), 2.04–2.01 (m, 1H, CH), 1.83–1.62 (m, 4H, CH,  $CH_3$ ), 1.27 (m, 3H,  $CH_3$ );  $^{13}C$  NMR ( $CDCl_3$ , 100 MHz):  $\delta$  172.3, 153.9, 137.4, 130.7, 127.8, 110.7, 110.6, 109.0, 108.7, 102.5, 58.5, 55.8, 36.6, 27.3, 23.0, 20.4, 18.8, 17.7, 16.8, 14.4; HRMS (ESI-TOF)  $m/z$ :  $[M + H]^+$  calcd for  $C_{20}H_{26}NO_4$ , 344.1862 found, 346.1865.

■ **DIMETHYL**  
**2-(6,7,8,9-TETRAHYDRO-3-ISOPROPYL-5H-CARBAZOL-7YL)-2-METHYLMALONATE 5H**

Half-white solid; mp 130–131 °C.  $^1H$  NMR ( $CDCl_3$ , 400 MHz):  $\delta$  7.70 (s, 1H, NH), 7.32 (s, 1H, Ar-H), 7.12–7.10 (d,  $J = 8.52$  Hz, 1H, Ar-H), 6.64–6.60 (m, 1H, Ar-H), 3.76 (s, 3H, OMe), 3.75 (s, 3H, OMe), 3.33–3.27 (m, 1H, CH), 2.69–2.50 (m, 5H, CH,  $(CH_2)_2$ ), 2.04–2.06 (m, 1H, CH), 1.69–1.53 (m, 4H, CH,  $CH_3$ ), 1.30 (s, 3H,  $CH_3$ ), 1.26 (s, 3H,  $CH_3$ );  $^{13}C$  NMR ( $CDCl_3$ , 100 MHz):  $\delta$  171.9, 153.2, 138.4, 131.2, 127.4, 111.5, 109.6, 108.1, 107.2, 103.5, 58.1, 52.9, 48.8, 39.4, 33.3, 23.4, 25.6, 24.9, 21.0, 16.9. HRMS (ESI-TOF)  $m/z$ :  $[M + H]^+$  calcd for  $C_{21}H_{28}NO_4$ , 358.2018 found, 358.2019.

■ **DIMETHYL**  
**2-(3-CYANO-6,7,8,9-TETRAHYDRO-5H-CARBAZOL-7YL)-2-METHYLMALONATE 5I**

Yellow solid; mp 120–121 °C.  $^1H$  NMR ( $CDCl_3$ , 400 MHz):  $\delta$  8.25 (s, 1H, NH), 7.82 (s, 1H, Ar-H), 7.78–7.75 (dd,  $J_1 = 4.4$  Hz,  $J_2 = 4.0$  Hz, 1H, Ar-H), 7.67–7.62 (m, 1H, Ar-H), 3.76 (s, 3H, OMe), 3.74 (s, 3H, OMe), 2.82–2.66 (m, 5H, CH,  $(CH_2)_2$ ), 2.05–2.01 (m, 1H, CH), 1.57–1.49 (m, 4H, CH,  $CH_3$ ).  $^{13}C$  NMR ( $CDCl_3$ , 100 MHz):  $\delta$  171.9, 153.2, 138.4, 131.2, 127.4, 118.5, 111.5, 109.6, 108.1, 107.2, 103.5, 58.1, 52.9, 39.4, 23.4, 24.9, 21.0, 17.7, 16.8. HRMS (ESI-TOF)  $m/z$ :  $[M + H]^+$  calcd for  $C_{19}H_{21}N_2O_4$ , 341.1501 found, 341.1503.

■ **DIMETHYL**  
**2-(3-NITRO-6,7,8,9-TETRAHYDRO-5H-CARBAZOL-7YL)-2-METHYLMALONATE 5J**

Brown solid; mp 135–136 °C.  $^1H$  NMR ( $CDCl_3$ , 400 MHz):  $\delta$  8.31 (s, 1H, NH), 8.01–7.98 (d,  $J = 12.0$  Hz, 1H, Ar-H), 7.75–7.72 (d,  $J = 12.0$  Hz, 1H, Ar-H), 7.67–7.64 (m, 1H, Ar-H), 3.77 (s, 3H, OMe), 3.75 (s, 3H, OMe), 2.84–2.63 (m, 5H, CH,  $(CH_2)_2$ ), 2.07–2.02 (m, 1H, CH), 1.59–1.50 (m, 4H, CH,  $CH_3$ );  $^{13}C$  NMR ( $CDCl_3$ , 100 MHz):  $\delta$  173.0, 172.5, 152.5, 135.0, 132.1, 110.4, 110.1, 109.2, 108.4, 103.6, 57.3, 52.2, 52.2, 39.4, 25.4, 25.1, 21.0, 16.1; HRMS (ESI-TOF)  $m/z$ :  $[M + H]^+$  calcd for  $C_{18}H_{21}N_2O_6$ , 361.1400 found, 361.1402.

■ **ASSOCIATED CONTENT**

SI **Supporting Information**

The Supporting Information is available free of charge at <https://pubs.acs.org/doi/10.1021/acsomega.0c06345>.

Materials used in the study, SiRNA sequences (Table S1), reaction conditions for the synthesis of compounds (Table S2), composition of the NQO1 assay cocktail (Table S3), ORTEP diagram of **5a** (Figure S1), and NQO1 activity calculation (PDF)

■ **AUTHOR INFORMATION**

**Corresponding Authors**

**Basappa** – Laboratory of Chemical Biology, Department of Studies in Organic Chemistry, University of Mysore, Mysore 570005, Karnataka, India; [orcid.org/0000-0002-6810-9219](https://orcid.org/0000-0002-6810-9219); Phone: +91-948-120-0076; Email: [salundibasappa@gmail.com](mailto:salundibasappa@gmail.com)

**SubbaRao V. Madhunapantula** – Department of Biochemistry (DST-FIST Supported Department), JSS Medical College and Special Interest Group in Cancer Biology and Cancer Stem Cells (SIG-CBCSC), JSS Academy of Higher Education & Research, Mysore 570015, Karnataka, India; [orcid.org/0000-0001-9167-9271](https://orcid.org/0000-0001-9167-9271); Phone: +91-810-527-8621; Email: [mvsstsubbarao@jssuni.edu.in](mailto:mvsstsubbarao@jssuni.edu.in)

**Authors**

**Prathima Chikkegowda** – Department of Pharmacology, JSS Medical College, JSS Academy of Higher Education & Research, Mysore 570015, Karnataka, India

**Baburajeev C. Pookunoth** – Laboratory of Chemical Biology, Department of Studies in Organic Chemistry, University of Mysore, Mysore 570005, Karnataka, India

**Venugopal R. Bovilla** – Department of Biochemistry (DST-FIST Supported Department), JSS Medical College and Center of Excellence in Molecular Biology and Regenerative Medicine (CEMR, DST-FIST Supported Center), JSS Medical College, JSS Academy of Higher Education & Research, Mysore 570015, Karnataka, India

**Prashanthkumar M. Veeresh** – Department of Biochemistry (DST-FIST Supported Department), JSS Medical College and Center of Excellence in Molecular Biology and Regenerative Medicine (CEMR, DST-FIST Supported Center), JSS Medical College, JSS Academy of Higher Education & Research, Mysore 570015, Karnataka, India

**Zonunsiami Leihang** – Department of Biochemistry (DST-FIST Supported Department), JSS Medical College and Center of Excellence in Molecular Biology and Regenerative Medicine (CEMR, DST-FIST Supported Center), JSS

Medical College, JSS Academy of Higher Education & Research, Mysore 570015, Karnataka, India

**Thippeswamy Thippeswamy** – Department of General Medicine, JSS Medical College and Hospital, JSS Academy of Higher Education & Research, Mysore 570015, Karnataka, India

**Mahesh A. Padukudru** – Department of Respiratory Medicine, JSS Medical College, and Hospital, JSS Academy of Higher Education & Research, Mysore 570015, Karnataka, India

**Basavanagowdappa Hathur** – Center of Excellence in Molecular Biology and Regenerative Medicine (CEMR, DST-FIST Supported Center), JSS Medical College, Department of General Medicine, JSS Medical College and Hospital, Faculty of Medicine, JSS Medical College and Hospital, JSS Medical College and Hospital, and Special Interest Group in Patient Care Management, JSS Medical College and Hospital, JSS Academy of Higher Education & Research, Mysore 570015, Karnataka, India

**Rangappa S. Kanchugarakoppal** – Department of Studies in Chemistry, University of Mysore, Mysore 570005, Karnataka, India

Complete contact information is available at:

<https://pubs.acs.org/10.1021/acsomega.0c06345>

#### Author Contributions

<sup>††</sup>P.C., B.C.P., and V.R.B. contributed equally to this work.

#### Notes

The authors declare no competing financial interest.

#### ACKNOWLEDGMENTS

The authors would like to acknowledge the infrastructure support provided by the Department of Science & Technology to CEMR Laboratory (CR-FST-LS-1/2018/178) and to the Department of Biochemistry (SR/FST/LS-1-539/2012), the laboratory facilities provided by CEMR Laboratory, Department of Biochemistry, and Special Interest Group in Cancer Biology and Cancer Stem Cells (SIG-CBCSC), and JSS Academy of Higher Education & Research (Mysore, Karnataka, India). V.R.B. acknowledges the Post-doctoral Fellowship from Global Health Equity Scholars (GHES) fellowship program of NIH Fogarty International Center (Award no. D43 TW010540). V.R.B. and P.M.V. are grateful to the Indian Council of Medical Research (ICMR), Government of India for the Senior Research Fellowship (SRF) award. Z.L. thanks the Ministry of Tribal Affairs, Government of India for the award of National Fellowship and Scholarship for Higher Education of ST Students (NFST). Dr. Basappa thanks DBT-NER and VGST for funding.

#### REFERENCES

- Bray, F.; Ferlay, J.; Soerjomataram, I.; Siegel, R. L.; Torre, L. A.; Jemal, A. Global cancer statistics 2018: GLOBOCAN estimates of incidence and mortality worldwide for 36 cancers in 185 countries. *Ca-Cancer J. Clin.* **2018**, *68*, 394–424.
- Haggard, F. A.; Boushey, R. P. Colorectal cancer epidemiology: incidence, mortality, survival, and risk factors. *Clin. Colon Rectal Surg.* **2009**, *22*, 191–197.
- Arnold, M.; Sierra, M. S.; Laversanne, M.; Soerjomataram, I.; Jemal, A.; Bray, F. Global patterns and trends in colorectal cancer incidence and mortality. *Gut* **2017**, *66*, 683–691.
- Jemal, A.; Siegel, R.; Xu, J.; Ward, E. Cancer statistics, 2010. *Ca-Cancer J. Clin.* **2010**, *60*, 277–300.

(5) You, Y. N.; Xing, Y.; Feig, B. W.; Chang, G. J.; Cormier, J. N. Young-onset colorectal cancer: is it time to pay attention? *Arch. Intern. Med.* **2012**, *172*, 287–289.

(6) Oxnard, G. R.; Morris, M. J.; Hodi, F. S.; Baker, L. H.; Kris, M. G.; Venook, A. P.; Schwartz, L. H. When progressive disease does not mean treatment failure: reconsidering the criteria for progression. *J. Natl. Cancer Inst.* **2012**, *104*, 1534–1541.

(7) Nagpal, M.; Singh, S.; Singh, P.; Chauhan, P.; Zaidi, M. A. Tumor markers: A diagnostic tool. *Natl. J. Maxillofac Surg.* **2016**, *7*, 17–20.

(8) Tanaka, T. Colorectal carcinogenesis: Review of human and experimental animal studies. *J. Carcinog.* **2009**, *8*, No. 5.

(9) Braun, M. S.; Seymour, M. T. Balancing the efficacy and toxicity of chemotherapy in colorectal cancer. *Ther. Adv. Med. Oncol.* **2011**, *3*, 43–52.

(10) Tol, J.; Punt, C. J. Monoclonal antibodies in the treatment of metastatic colorectal cancer: a review. *Clin. Ther.* **2010**, *32*, 437–453.

(11) Yen, L. C.; Uen, Y. H.; Wu, D. C.; Lu, C. Y.; Yu, F. J.; Wu, I. C.; Lin, S. R.; Wang, J. Y. Activating KRAS mutations and overexpression of epidermal growth factor receptor as independent predictors in metastatic colorectal cancer patients treated with cetuximab. *Ann. Surg.* **2010**, *251*, 254–260.

(12) Jeong, W. S.; Jun, M.; Kong, A. N. Nrf2: a potential molecular target for cancer chemoprevention by natural compounds. *Antioxid. Redox Signaling* **2006**, *8*, 99–106.

(13) No, J. H.; Kim, Y. B.; Song, Y. S. Targeting nrf2 signaling to combat chemoresistance. *J. Cancer Prev.* **2014**, *19*, 111–117.

(14) Xiang, M.; Namani, A.; Wu, S.; Wang, X. Nrf2: bane or blessing in cancer? *J. Cancer Res. Clin. Oncol.* **2014**, *140*, 1251–1259.

(15) Itoh, K.; Mimura, J.; Yamamoto, M. Discovery of the negative regulator of Nrf2, Keap1: a historical overview. *Antioxid. Redox Signaling* **2010**, *13*, 1665–1678.

(16) Taguchi, K.; Motohashi, H.; Yamamoto, M. Molecular mechanisms of the Keap1-Nrf2 pathway in stress response and cancer evolution. *Genes Cells* **2011**, *16*, 123–140.

(17) Tonelli, C.; Chio, I. I. C.; Tuveson, D. A. Transcriptional Regulation by Nrf2. *Antioxid. Redox Signaling* **2018**, *29*, 1727–1745.

(18) Nguyen, T.; Nioi, P.; Pickett, C. B. The Nrf2-antioxidant response element signaling pathway and its activation by oxidative stress. *J. Biol. Chem.* **2009**, *284*, 13291–13295.

(19) Itoh, K.; Chiba, T.; Takahashi, S.; Ishii, T.; Igarashi, K.; Katoh, Y.; Oyake, T.; Hayashi, N.; Satoh, K.; Hatayama, I.; Yamamoto, M.; Nabeshima, Y. An Nrf2/small Maf heterodimer mediates the induction of phase II detoxifying enzyme genes through antioxidant response elements. *Biochem. Biophys. Res. Commun.* **1997**, *236*, 313–322.

(20) Sun, Z.; Zhang, S.; Chan, J. Y.; Zhang, D. D. Keap1 controls postinduction repression of the Nrf2-mediated antioxidant response by escorting nuclear export of Nrf2. *Mol. Cell. Biol.* **2007**, *27*, 6334–6349.

(21) Kansanen, E.; Kuosmanen, S. M.; Leinonen, H.; Levonen, A. L. The Keap1-Nrf2 pathway: Mechanisms of activation and dysregulation in cancer. *Redox Biol.* **2013**, *1*, 45–49.

(22) Hayes, J. D.; McMahon, M.; Chowdhry, S.; Dinkova-Kostova, A. T. Cancer chemoprevention mechanisms mediated through the Keap1-Nrf2 pathway. *Antioxid. Redox Signaling* **2010**, *13*, 1713–1748.

(23) Rojo de la Vega, M.; Chapman, E.; Zhang, D. D. NRF2 and the Hallmarks of Cancer. *Cancer Cell* **2018**, *34*, 21–43.

(24) Panieri, E.; Saso, L. Potential Applications of NRF2 Inhibitors in Cancer Therapy. *Oxid. Med. Cell. Longevity* **2019**, *2019*, No. 8592348.

(25) Wu, S.; Lu, H.; Bai, Y. Nrf2 in cancers: A double-edged sword. *Cancer Med.* **2019**, *8*, 2252–2267.

(26) Hayes, J. D.; McMahon, M. The double-edged sword of Nrf2: subversion of redox homeostasis during the evolution of cancer. *Mol. Cell* **2006**, *21*, 732–734.

(27) Lau, A.; Villeneuve, N. F.; Sun, Z.; Wong, P. K.; Zhang, D. D. Dual roles of Nrf2 in cancer. *Pharmacol. Res.* **2008**, *58*, 262–270.



- (28) Jaramillo, M. C.; Zhang, D. D. The emerging role of the Nrf2-Keap1 signaling pathway in cancer. *Genes Dev.* **2013**, *27*, 2179–2191.
- (29) Kensler, T. W.; Wakabayashi, N. Nrf2: friend or foe for chemoprevention? *Carcinogenesis* **2010**, *31*, 90–99.
- (30) Geismann, C.; Arlt, A.; Sebens, S.; Schafer, H. Cytoprotection “gone astray”: Nrf2 and its role in cancer. *OncoTargets Ther.* **2014**, *7*, 1497–1518.
- (31) Basak, P.; Sathukhan, P.; Sarkar, P.; Sil, P. C. Perspectives of the Nrf-2 signaling pathway in cancer progression and therapy. *Toxicol. Rep.* **2017**, *4*, 306–318.
- (32) Patel, B. B.; Sengupta, R.; Qazi, S.; Vachhani, H.; Yu, Y.; Rishi, A. K.; Majumdar, A. P. Curcumin enhances the effects of 5-fluorouracil and oxaliplatin in mediating growth inhibition of colon cancer cells by modulating EGFR and IGF-1R. *Int. J. Cancer* **2008**, *122*, 267–273.
- (33) Liu, Z.; Larock, R. C. Synthesis of Carbazoles and Dibenzofurans via Cross-Coupling of o-Iodoanilines and o-Iodophenols with Silylaryl Triflates and Subsequent Pd-Catalyzed Cyclization. *Tetrahedron* **2007**, *63*, 347–355.
- (34) Nandy, B. C.; Gupta, A. K.; Mittal, A.; Vyas, V. Carbazole: it's Biological Activity. *J. Biomed. Pharm. Res.* **2014**, *3*, 42–48.
- (35) Hou, S.; Yi, Y. W.; Kang, H. J.; Zhang, L.; Kim, H. J.; Kong, Y.; Liu, Y.; Wang, K.; Kong, H. S.; Grindrod, S.; Bae, I.; Brown, M. L. Novel carbazole inhibits phospho-STAT3 through induction of protein-tyrosine phosphatase PTPN6. *J. Med. Chem.* **2014**, *57*, 6342–6353.
- (36) Chang, L. C.; Tsao, L. T.; Chang, C. S.; Chen, C. J.; Huang, L. J.; Kuo, S. C.; Lin, R. H.; Wang, J. P. Inhibition of nitric oxide production by the carbazole compound LCY-2-CHO via blockade of activator protein-1 and CCAAT/enhancer-binding protein activation in microglia. *Biochem. Pharmacol.* **2008**, *76*, 507–519.
- (37) Zhang, M.; Wang, B.; Chong, Q. Y.; Pandey, V.; Guo, Z.; Chen, R. M.; Wang, L.; Wang, Y.; Ma, L.; Kumar, A. P.; Zhu, T.; Wu, Z. S.; Yin, Z.; Basappa; Goh, B. C.; Lobie, P. E. A novel small-molecule inhibitor of trefoil factor 3 (TFF3) potentiates MEK1/2 inhibition in lung adenocarcinoma. *Oncogenesis* **2019**, *8*, No. 65.
- (38) Pandey, V.; Wang, B.; Mohan, C. D.; Raquib, A. R.; Rangappa, S.; Srinivasa, V.; Fuchs, J. E.; Girish, K. S.; Zhu, T.; Bender, A.; Ma, L.; Yin, Z.; Basappa; Rangappa, K. S.; Lobie, P. E. Discovery of a small-molecule inhibitor of specific serine residue BAD phosphorylation. *Proc. Natl. Acad. Sci. U.S.A.* **2018**, *115*, E10505–E10514.
- (39) Rakesh, K. S.; Jagadish, S.; Vinayaka, A. C.; Hemshekhar, M.; Paul, M.; Thushara, R. M.; Sundaram, M. S.; Swaroop, T. R.; Mohan, C. D.; Basappa; Sadashiva, M. P.; Kemparaju, K.; Girish, K. S.; Rangappa, K. S. A new ibuprofen derivative inhibits platelet aggregation and ROS mediated platelet apoptosis. *PLoS One* **2014**, *9*, No. e107182.
- (40) Ren, Y.-M.; Cai, C.; Yang, R.-C. Molecular iodine-catalyzed multicomponent reactions: an efficient catalyst for organic synthesis. *RSC Adv.* **2013**, *3*, 7182–7204.
- (41) Wang, X. S.; Yang, K.; Zhou, J.; Tu, S. J. Facile method for the combinatorial synthesis of 2,2-disubstituted quinazolin-4(1H)-one derivatives catalyzed by iodine in ionic liquids. *J. Comb. Chem.* **2010**, *12*, 417–421.
- (42) Chu, C. M.; Gao, S.; Sastry, M. N. V.; Yao, C. F. Iodine-catalyzed Michael addition of mercaptans to  $\alpha,\beta$ -unsaturated ketones under solvent-free conditions. *Tetrahedron Lett.* **2005**, *46*, 4971–4974.
- (43) Ma, Q. Role of nrf2 in oxidative stress and toxicity. *Annu. Rev. Pharmacol. Toxicol.* **2013**, *53*, 401–426.
- (44) Moon, J.; Yu, S. J.; Kim, H. S.; Sohn, J. Induction of G(1) cell cycle arrest and p27(KIP1) increase by panaxydol isolated from Panax ginseng. *Biochem. Pharmacol.* **2000**, *59*, 1109–1116.
- (45) Fofaria, N. M.; Ranjan, A.; Kim, S. H.; Srivastava, S. K. Mechanisms of the Anticancer Effects of Isothiocyanates. *Enzymes* **2015**, *37*, 111–137.
- (46) Jaganjac, M.; Milkovic, L.; Sunjic, S. B.; Zarkovic, N. The NRF2, Thioredoxin, and Glutathione System in Tumorigenesis and Anticancer Therapies. *Antioxidants* **2020**, *9*, No. 1151.
- (47) Homma, S.; Ishii, Y.; Morishima, Y.; Yamadori, T.; Matsuno, Y.; Haraguchi, N.; Kikuchi, N.; Satoh, H.; Sakamoto, T.; Hizawa, N.; Itoh, K.; Yamamoto, M. Nrf2 enhances cell proliferation and resistance to anticancer drugs in human lung cancer. *Clin. Cancer Res.* **2009**, *15* (10), 3423–3432.
- (48) Mishra, S.; Tamta, A. K.; Sarikhani, M.; Desingu, P. A.; Kizkekra, S. M.; Pandit, A. S.; Kumar, S.; Khan, D.; Raghavan, S. C.; Sundaresan, N. R. Subcutaneous Ehrlich Ascites Carcinoma mice model for studying cancer-induced cardiomyopathy. *Sci. Rep.* **2018**, *8*, No. 5599.
- (49) Vijay Avin, B. R.; Thirusangu, P.; Lakshmi Ranganatha, V.; Firdouse, A.; Prabhakar, B. T.; Khanum, S. A. Synthesis and tumor inhibitory activity of novel coumarin analogs targeting angiogenesis and apoptosis. *Eur. J. Med. Chem.* **2014**, *75*, 211–221.
- (50) Sujatha, P.; Anantharaju, P. G.; Veeresh, P. M.; Dey, S.; Bovilla, V. R.; Madhunapantula, S. R. V. Diallyl Disulfide (DADS) Retards the Growth of Breast Cancer Cells in Vitro and in Vivo Through Apoptosis Induction. *Biomed. Pharmacol. J.* **2017**, *10*, 1619–1630.
- (51) Bovilla, V. R.; Anantharaju, P. G.; Dornadula, S.; Veeresh, P. M.; Kuruburu, M. G.; Bettada, V. G., et al. Caffeic acid and protocatechuic acid modulate Nrf2 and inhibit Ehrlich ascites carcinomas in mice. *Asian Pac. J. Trop. Biomed.* **2021**, *11*, in press.
- (52) Jayanthi, M. K. Screening and Identification of Plant Extracts for Inhibiting Lung Cancer Cell Line Expressing Elevated NRF2 Signaling. Thesis, 2017.
- (53) Sadashiva, M. P.; Basappa; NanjundaSwamy, S.; Li, F.; Manu, K. A.; Sengottavelan, M.; Prasanna, D. S.; Anilkumar, N. C.; Sethi, G.; Sugahara, K.; Rangappa, K. S. Anti-cancer activity of novel dibenzo[b,f]azepine tethered isoxazoline derivatives. *BMC Chem. Biol.* **2012**, *12*, No. 5.
- (54) Prochaska, H. J.; Santamaria, A. B.; Talalay, P. Rapid detection of inducers of enzymes that protect against carcinogens. *Proc. Natl. Acad. Sci. U.S.A.* **1992**, *89*, 2394–2398.
- (55) Prochaska, H. J.; Santamaria, A. B. Direct measurement of NAD(P)H:quinone reductase from cells cultured in microtiter wells: a screening assay for anticarcinogenic enzyme inducers. *Anal. Biochem.* **1988**, *169*, 328–336.
- (56) Madhunapantula, S. V.; Desai, D.; Sharma, A.; Huh, S. J.; Amin, S.; Robertson, G. P. PBiSe, a novel selenium-containing drug for the treatment of malignant melanoma. *Mol. Cancer Ther.* **2008**, *7*, 1297–1308.
- (57) Chomczynski, P.; Sacchi, N. The single-step method of RNA isolation by acid guanidinium thiocyanate-phenol-chloroform extraction: twenty-something years on. *Nat. Protoc.* **2006**, *1*, 581–585.
- (58) Aranda, P. S.; LaJoie, D. M.; Jorczyk, C. L. Bleach gel: a simple agarose gel for analyzing RNA quality. *Electrophoresis* **2012**, *33*, 366–369.
- (59) Madhunapantula, S. V.; Sharma, A.; Robertson, G. P. PRAS40 deregulates apoptosis in malignant melanoma. *Cancer Res.* **2007**, *67*, 3626–3636.
- (60) Walker, J. M. The bicinchoninic acid (BCA) assay for protein quantitation. *Methods Mol. Biol.* **1994**, *32*, 5–8.
- (61) Baghirova, S.; Hughes, B. G.; Hendzel, M. J.; Schulz, R. Sequential fractionation and isolation of subcellular proteins from tissue or cultured cells. *MethodsX* **2015**, *2*, 440–445.
- (62) Shailasree, S.; Venkataramana, M.; Niranjana, S. R.; Prakash, H. S. Cytotoxic effect of p-Coumaric acid on neuroblastoma, N2a cell via generation of reactive oxygen species leading to dysfunction of mitochondria inducing apoptosis and autophagy. *Mol. Neurobiol.* **2015**, *51*, 119–130.
- (63) Rok, J.; Rzepka, Z.; Beberok, A.; Pawlik, J.; Wrzesniok, D. Cellular and Molecular Aspects of Anti-Melanoma Effect of Minocycline-A Study of Cytotoxicity and Apoptosis on Human Melanotic Melanoma Cells. *Int. J. Mol. Sci.* **2020**, *21*, No. 6917.
- (64) Chodkowski, M.; Serafinska, I.; Brzezicka, J.; Banbura, M. W.; Cymerys, J. Application of NucleoCounter for the comprehensive assessment of murine cultured neurons during infection with Equine Herpesvirus type 1 (EHV-1). *Pol. J. Vet. Sci.* **2017**, *20*, 831–834.

(65) Beberok, A.; Wrzesniok, D.; Szlachta, M.; Rok, J.; Rzepka, Z.; Respondek, M.; Buszman, E. Lomefloxacin Induces Oxidative Stress and Apoptosis in COLO829 Melanoma Cells. *Int. J. Mol. Sci.* **2017**, *18*, No. 2194.

(66) Beberok, A.; Wrzesniok, D.; Rok, J.; Rzepka, Z.; Respondek, M.; Buszman, E. Ciprofloxacin triggers the apoptosis of human triple-negative breast cancer MDA-MB-231 cells via the p53/Bax/Bcl-2 signaling pathway. *Int. J. Oncol.* **2018**, *52*, 1727–1737.

(67) Sunila, E. S.; Kuttan, G. Immunomodulatory and antitumor activity of *Piper longum* Linn. and piperine. *J. Ethnopharmacol.* **2004**, *90*, 339–346.

(68) Strober, W. Trypan Blue Exclusion Test of Cell Viability. *Curr. Protoc. Immunol.* **2015**, *111*, A3.B.1–A3.B.3.

(69) Jonsson, M.; Jestoi, M.; Nathanail, A. V.; Kokkonen, U. M.; Anttila, M.; Koivisto, P.; Karhunen, P.; Peltonen, K. Application of OECD Guideline 423 in assessing the acute oral toxicity of moniliformin. *Food Chem. Toxicol.* **2013**, *53*, 27–32.